ACS EARTH AND SPACE CHEMISTRY

http://pubs.acs.org/journal/aesccq

Article

Investigating Spatial Heterogeneity in Aerosols Chemical Composition and Implications for Physico-Optical Properties over the North Eastern Region of India

Binita Pathak,* Barlin Das, Partha Jyoti Sahu, Mukunda Madhab Gogoi, Pradip Kumar Bhuyan, Krishnanka Jyoti Baishya, Pranami Mahanta, Kalyan Bhuyan, Jhuma Biswas, Rumajyoti Hazarika, Saradi Bora, Malabika Borah, Romesh Borgohain, Jagannath Bhuyan, Kakali Bhuyan, and Swapnali Hazarika

Cite This: https://doi.org/10.1021/acsearthspacechem.5c00197

Read Online

ACCESS | Metrics & More | Article Recommendations | Supporting Information

ABSTRACT: Total suspended particulates (TSP) samples were collected using a high-volume sampler in a campaign mode observation over seven selected locations in North-East India, during post-monsoon season of 2023. Scanning electron microscopy (SEM) and energy-dispersive X-ray (EDX) system analysis have been performed to understand the morphology, size, and elemental composition of ambient TSP. EDX analysis reveals the presence of C, O, Mg, Si, Na, Al, and K as the significant elements in almost all the samples, and Cr, Cu, Zn, Fe, P, S, Ti, and Ba as minor elements in some of the samples, posing possible threats to human health. These particles are classified into three groups: biogenic, geogenic, and anthropogenic based on the elemental spectrum and morphological features. Fourier Transform Infrared Spectroscopic analysis shows consistent chemical constituents, including calcite, silicate, palygorskite, Illite, and aliphatic hydrocarbons across all the sampling locations. Integrated source apportionment studies like the Enrichment Factor, Pearson Correlation Coefficient, and Principal Component Analysis reveal a mixed source of aerosols originating from both crustal and industrial origins in the eastern part. In contrast, industrial and vehicular emissions primarily influence the middle sector and the western part. SEM analysis confirmed the existence of a wide range of particles with diverse morphologies, mainly spherical and irregular shapes such as rectangles, discs, and cone-like forms, in aerosols across the region, with an abundance of Si. The Discrete Dipole Approximation is further used to simulate the optical properties of these aerosols, considering dust as the constituent but with varying shapes and sizes.

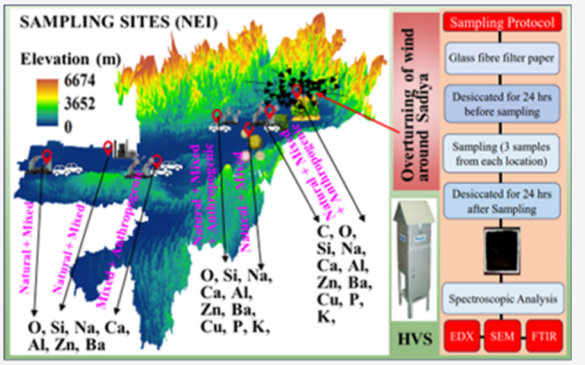

KEYWORDS: *North-East India, aerosol chemical analysis, enrichment factor, principal component analysis, DDSCAT, climate action, pollution control*

1. INTRODUCTION

The total suspended particulates (TSP) or particulate matter (PM) comprises a wide range of constituents that exhibit variations both at the local and regional levels. Their impact on radiation, climate change, and human well-being demands a thorough exploration of aerosol particles, focusing on their composition, sources, transport, and fate.[1] Understanding the composition of TSP involves examining the origins of its components and analyzing their particle sizes. Application of energy dispersive spectrometry (EDX) combined with scanning electron microscopy (SEM) can reveal important details about the size, shape, and elemental information on PM and thus help to identify their different sources.[2−6] Several studies have been carried out, particularly in urban regions around the globe, on aerosol morphology and related elemental composition measurements.[7−10] In the Indian subcontinent, Elemental characterization has been carried out mainly using SEM−EDX analysis,[6,11−14] but the studies related to single particle spectrum analysis of atmospheric PM are relatively sparse.[15−17]

The investigation of the radiative[18] and chemical[19−21] properties of PM in terms of the morphology and elemental analyses has drawn more attention in recent years. PM in the atmosphere significantly impacts climate, as evidenced by

Received: July 27, 2025
Revised: November 14, 2025
Accepted: November 19, 2025

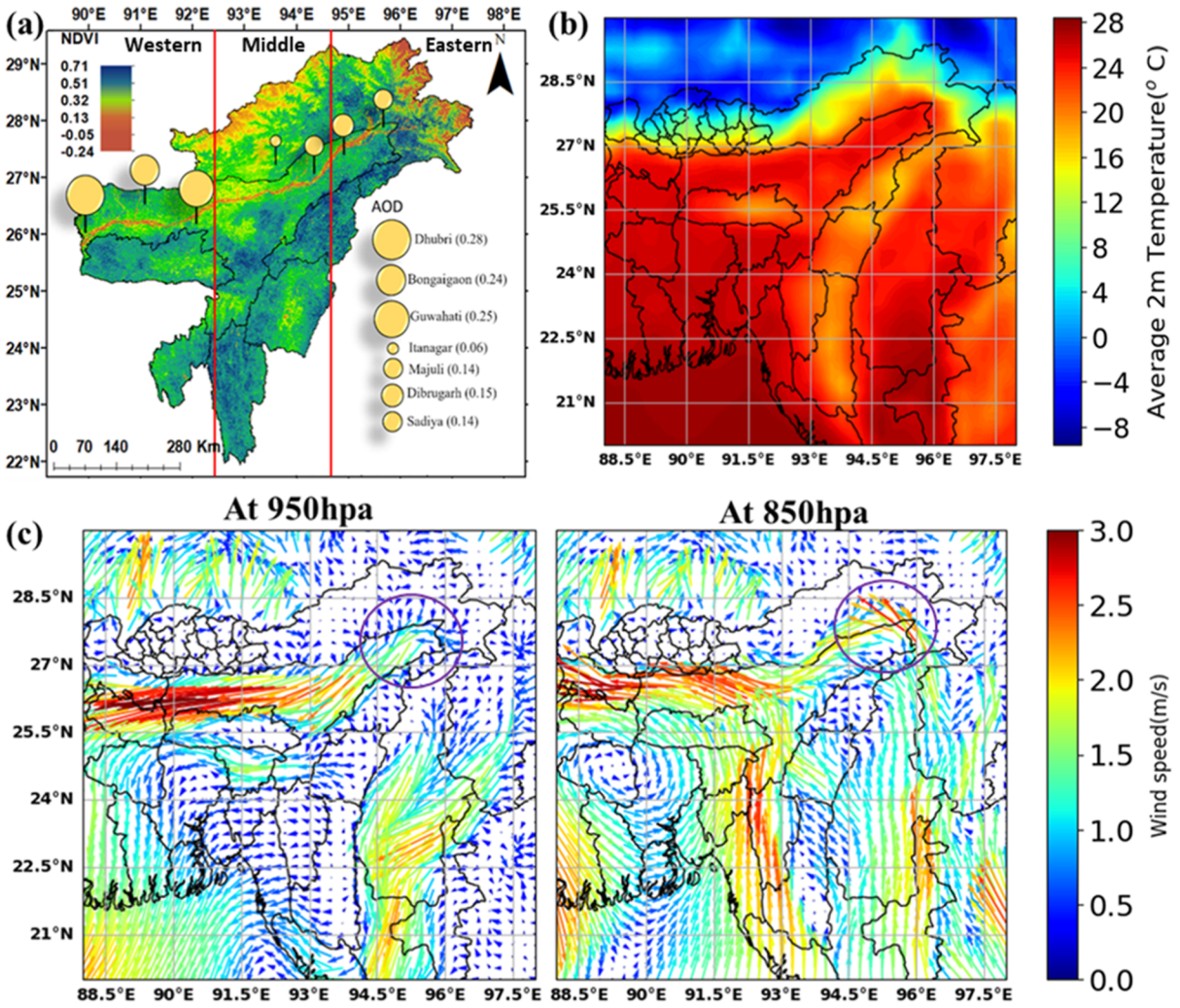

Figure 1. (a) Normalized difference vegetation index (NDVI) map of NEI, where the bubbles represents the MODIS retrieved AOD during the post-monsoon season, 2023 over the sampling locations: Dhubri (26.0°N, 89.1°E, 30 m amsl), Bongaigaon (26.3°N, 90.3°E, 40 m amsl), Guwahati (26.2°N, 91.7°E, 53 m amsl) in the western sector (89.97°−92.45°E), Itanagar (27.1°N, 93.7°E, 350 m amsl) and Majuli (27.0°N, 94.1°E, 75 amsl) in middle sector (92.45°−94.63°E) and Dibrugarh (27.4°N, 94.8°E, 111m amsl), and Sadiya (27.9°N, 95.8°E, 26 m amsl) in the eastern sector (94.63°−95.55°E), (b) average 2m temperature, and (c) average wind speed at 950 hPa and 850 hPa from over NEI during post monsoon season, 2023.

global simulations and measurements of direct radiative forcing from anthropogenic and nonanthropogenic aerosols.[22] When humidified, particles with dissimilar morphology might transform into a spherical shape. A common assumption in many applications is that atmospheric particles are spherical, overlooking the presence of various morphologies, such as fibers, platelets, and isometric particles.[23] Nonspherical aerosols, such as dust and soot, often have complex shapes that influence their optical properties differently than spheres.[24] This assumption can lead to errors in estimating the angular distribution of scattered light, polarization, and absorption efficiency, which in turn affect climate models and remote sensing data.[25] For instance, Mishchenko et al. (1999)[26] highlighted that spherical assumptions could lead to substantial errors in radiative forcing calculations, particularly for aerosols like mineral dust and volcanic ash.[27] Overall, the assumption of sphericity in radiative transfer models can introduce uncertainties in radiative forcing estimates, typically ranging from 20 to 50%[28−30] depending on the type of aerosol and its actual shape. Okada et al. (2010)[31] reviewed various computer techniques for calculating single-scattering properties of large fluffy nonspherical particles, including codes based on the Discrete Dipole Approximation (DDA) method proposed by Purcell and Pennypacker (1973).[32] It was further developed by Draine (1988),[33] along with a variant of the T-matrix code for fixed scatter orientation. In both cases, orientation averaging is done quantitatively. This reduces the need for computer memory while increasing the time to execute code. DDA can simulate particles of any shape, including irregular, nonspherical, or fractal shapes found in air aerosols such as mineral dust, soot, and biological particles. Unlike simpler approaches such as Mie theory, which assumes sphericity, DDA yields accurate conclusions for particles with complicated geometries. Discrete Dipole scattering (DDSCAT), an implementation of DDA, is chosen in the present study to estimate the optical properties of aerosols because it allows for exact and flexible modeling of complex, nonspherical particles, which is vital for understanding the actual optical behavior of aerosols in the atmosphere. However, to fully realize the potential of

https://doi.org/10.1021/acsearthspacechem.5c00197
ACS Earth Space Chem. XXXX, XXX, XXX−XXX

DDSCAT in advancing the retrieval of irregularly shaped atmospheric particles, there needs to be a convenient way of generating the "shape file" containing dipole configurations. This file serves as an input to predict the optical behavior of particles after visualizing their importance in approximating their morphology. Otherwise, numerical modeling may not be feasible within a realistic time scale.

The North-East India (NEI), encompassed by the eastern Himalayan foothills, provides ideal conditions for atmospheric chemistry, owing to abundant solar insolation and the presence of both local and anthropogenic aerosols, along with reactive trace gases. The dense forests and natural vegetation in the NEI region serve as key sources of volatile organic compounds (VOCs) and biological aerosols.[34,35] Additionally, it stands as a global hotspot for lightning activity, which notably contributes to elevated ozone (O_3) levels through the direct production of nitrogen oxides (NO_x),[36] a significant precursor of Secondary Organic Aerosols (SOA). The region's distinctive geography and terrain create ideal conditions for trapping both local and transported pollutants, leading to elevated levels of gases and particulates as reported in previous studies.[37−39] Extensive investigations have been carried out to characterize aerosols and assess their climatic implications in the Eastern Himalayan Foothills region, including NEI, using ground-based observations,[39−52] satellite data,[53−55] short-term campaigns,[56,57] and regional climate modeling.[58−62] NEI, as a global biodiversity hotspot with heterogeneous emission patterns and sources—including local biomass burning, industrial operations, and long-distance transportation from adjacent areas—and influenced by livelihood demand, is highly susceptible to variations in atmospheric composition. Aerosols released from both natural and anthropogenic sources play a critical role in regulating air quality and regional climate over this region. Campaign mode research aids in identifying the regional distribution of aerosols, supported by various emission sources. It enhances the spatial understanding of complex environmental processes through short-term, coordinated monitoring, capturing essential variations often lost in everyday observations. Such research is particularly crucial for understanding localized phenomena, validating models, and making appropriate policy decisions. The campaign mode investigation is critical in ecologically vulnerable and geographically challenging areas like NEI, which is noted for its peculiar biodiversity, fragile ecosystems, varied cultural landscape, and microclimatic variations. Earlier, Pathak et al. (2014)[56] demonstrated through campaign mode measurements that the Brahmaputra Valley exhibits significant spatial heterogeneity in aerosol loading, with higher PM_{10} and $PM_{2.5}$ concentrations in the western (89.97°−92.45°E) and middle sectors (92.5°−94.63°E) compared to the eastern sector (94.63°−95.55°E). Their findings further revealed a west-to-east decreasing gradient in black carbon (BC) concentrations, highlighting the influence of localized emission sources and atmospheric transport processes. Moreover, the Indian Space Research Organisation (ISRO) and Ministry of Earth Sciences (MoES) have carried out focused campaigns in NEI to observe monsoon variability and landslides, highlighting the necessity of targeted efforts owing to the region's rugged topography and rainfall variability.[63,64] Another campaign mode observation on bioaerosols[35,65] has observed distinct spatial and seasonal variability in abundance of viable microbes, pollen, fungal spores, and animal debris, underscoring the region's complex aerobiological interactions. However, a study to characterize the physico-optical properties through chemical composition observed over the region has not been addressed so far. Thus, the present study aims to investigate the aerosol types based on their chemical composition obtained through spectroscopic analysis techniques and to explore their links to physico-optical properties over seven distinct locations of NEI. Additionally, the study aims to identify the aerosol emission sources. Another key objective of the study is to model the behavior of nonspherical dust particles using DDSCAT. The simulated shape and size-dependent optical properties of dust aerosols are integral in further modeling the radiative properties of nonspherical particles, often approximating their real shapes.

2. STUDY REGION, DATA, AND METHODOLOGY

2.1. Study Region. The campaign mode observation was conducted in NEI at seven distinct locations across the eastern, middle, and western sectors. The sector of the west (89.97°−92.45°E) includes Dhubri, Bongaigaon, and Guwahati, the middle sector (92.45°−94.63°E) includes Itanagar and Majuli, while Dibrugarh and Sadiya are in the eastern sector (94.63°−95.55°E) (Figure 1a). The region experiences a subtropical humid climate with mild winters and hot summers, along with heavy monsoon rainfall. The monsoon retreats in the postmonsoon season, when the temperature of the region reaches up to 28 °C (Figure 1b). The wind pattern shifts from southeasterly in the summer monsoon to northwesterly in the winter monsoon. Owing to the scanty rainfall, the campaign was conducted during the post-monsoon season of 2023. The aerosol optical depth value is highest in the western sector, followed by the eastern sector. Dhubri (26.0°N, 89.1°E, 30 m amsl) is a semi-urban town in west Assam, situated on the banks of the Brahmaputra River (Figure 1a). The town is situated in an alluvial floodplain, where fertile soils provide support for large-scale agriculture and hence a high population density. Bongaigaon (26.3°N, 90.3°E, 40 m amsl) is a key industrial town in western Assam, known for its oil refinery and coal deposits, situated at the eastern border of the Shillong Plateau. It falls in the Brahmaputra floodplain, which includes alluvial and Tertiary sedimentary formations. Its presence of coal-bearing rocks gives it economic importance as an energy source. Guwahati (26.2°N, 91.7°E, 53 m amsl) is the largest city in NEI, situated in the Brahmaputra River valley and bounded by the Shillong Plateau to the south and the Himalayan foothills to the north. The town has expanded due to urbanization and industrialization in recent years, resulting in a high population density. Itanagar (27.1°N, 93.7°E, 350 m amsl), the capital of Arunachal Pradesh, is a semi-urban city located in the foothills of the Eastern Himalayas. The rugged terrain, steep slopes, and dense forests characterize it. Majuli (27.0°N, 94.1°E, 75 m amsl), the second-largest river island in the world, is an unusual and sensitive ecosystem in the Brahmaputra River. It is a countryside with dispersed populations and extensive wetlands. It is a highly dynamic island subject to ongoing erosion and sedimentation caused by changes in the channel course of the Brahmaputra. Dibrugarh (27.4°N, 94.6°E, 111 m amsl), located in the northeastern region of Assam, spans an area of 3381 km^2. Based on Land Use Land Cover (LULC) data,[52] the area comprises agricultural land (43.36%), tea gardens (21.07%), forest cover (11.4%), and river sand deposits (10.88%). The district is rich in natural resources, particularly crude oil and coal, which are concentrated in the eastern and southeastern parts. These resources are distributed across a 100 km radius around

https://doi.org/10.1021/acsearthspacechem.5c00197
ACS Earth Space Chem. XXXX, XXX, XXX−XXX

the central study area, making Dibrugarh a vital zone for energy production and economic development. Sadiya (27.9°N, 95.8°E, 26 m amsl) is a rural town in eastern Assam, surrounded by several tributaries of the Brahmaputra. The area is located within an active basin of sediment deposition, with continuous alluvial material deposition from upstream rivers. The near-surface wind patterns both at 950 hPa and 850 hPa obtained from ERA5 Land data reveal an overturning of wind around Sadiya (black circle in Figure 1c).

2.2. Sample Collection. A high-volume sampler (STAPLEX, TSP-2) was used to sample TSP on glass filter paper (8 × 10 in.) at a 1 m^3/min flow rate from 27th Oct to 8th Nov, 2023, during fair weather conditions. Three samples were collected from all the locations with a sampling period of 8 h for each sample. A glass filter is a "depth" filter that traps particles throughout its depth rather than on the surface (polycarbonate filter), making it suitable for efficient sample collection during short sampling periods. A flow meter was used to maintain the flow rate consistent. The sampler underwent regular cleaning and calibration. The instrument was set up on the rooftop of the building to expose it to the ambient air in all directions. Samples collected from each location in this manner are considered representative of the entire area because the sample duration is 24 h.

2.3. Quality Assurance. The filter paper was desiccated at 25 °C for 24 h before and after sampling to control the excess humidity. Field Blank was taken to be used as a reference for a particular location. A set of 3 samples was collected according to the sampling protocol, and mean blank values were deducted from the sample concentrations. Rainy days were avoided when collecting samples to protect the devices. To prevent volatile components from evaporating, the samples were sealed in an airtight polythene zip-lock bag and stored in a deep freezer at −4 °C until the analysis was completed.

2.4. Elemental and Morphological Analysis. Morphological and elemental analysis was performed using a SEM (JEOL JSM 6390 LV), an EDX, and an INCAx Sight microanalysis system (Oxford Instruments, model 7582). One cm^2 areas from each sample were analyzed at 120× magnification with a detection area of 1 mm^2. The EDX was fitted with a silicon (lithium drifting) crystal detector with an enhanced acquisition rate of 50,000 cps. A Super Atmosphere Supporting Thin Window (SATW), which assured good resolution on the low-energy end of the spectrum and, under specific conditions, allowed the chemical analysis of elements down to boron, was also featured in the detector. For the quant optimization purposes, high-purity Cu and Ni (99.99%) were used to ensure accurate elemental quantification in the sample. The detector has a minimum quantification limit of 0.01 wt %, with a resolution of 137 eV at 5.9 keV. The analytical method is based on Deka and Haque (2014)[12] and the references therein. Three areas were randomly selected for SEM and EDX examination from the corresponding sample filters. The results were quantified from the average of the three measurements, with a standard deviation of ±10%. Advanced algorithms in the software accounted for overlapping peaks and allowed proper quantification. INCA software performed background subtraction and peak identification with automatic adjustment by ZAF. It uses mass absorption coefficients, which account for the differences in the generation and absorption of X-rays concerning elements. The formula for calculating wt % is as follows

$$\text{wt}\%_i = \frac{I_i A_i}{\sum (I_j A_j)} \times 100 \tag{1}$$

where I_j is the corrected intensity, A_i is the atomic mass of element i, and the sum is over all elements j.

2.5. Estimation of Optical Properties. The DDSCAT v.7.3.3 is used to compute light scattering by dust aerosols, with shapes obtained from SEM−EDX analysis. The DDSCAT software package implements the DDA to compute the optical properties, such as scattering and absorption, through the interaction of electromagnetic waves with the target (dust aerosols in the present case) of variable geometries and complex refractive indices. Here, the target particles are replaced by an array of point dipoles (polarizable points) arranged in a lattice. This arrangement is designed to match the irregular shape of the particles using the realistic dust shape model obtained in SEM−EDX analysis. Draine (1988)[33] and Draine & Flatau (1994)[66] provided the theory and implementation of the DDA in DDSCAT, respectively.

The DDA is entirely adaptable in terms of target geometry. It requires minimal interdipole spacing (d) compared to structural lengths and wavelength (λ), satisfying the relationship

$$|m|kd < 1 \tag{2}$$

where m represents the target refractive index and $k = 2\pi/\lambda$ is the wave vector.

This condition is valid if $|m - 1| < 3$.

Let, N be the number of dipoles with interdipole spacing d, then the volume of the target material will be

$$V = Nd^3 \tag{3}$$

The effective radius (a_{eff}), which is the radius of an equal volume of a sphere, can be given as

$$a_{\text{eff}} = \left(\frac{3V}{4\pi}\right)^{1/3} \tag{4}$$

The associated size parameter x is represented as

$$x = ka_{\text{eff}} = \frac{2\pi}{\lambda}\left(\frac{3V}{4\pi}\right)^{1/3} \tag{5}$$

where $k = \frac{2\pi}{\lambda}$ is the wave vector.

The size parameter can be related to the number of dipoles, N, and $|m|kd$ as

$$x = \frac{62.04}{|m|}\left(\frac{N}{10^6}\right)^{1/3}|m|kd \tag{6}$$

Each dipole in DDSCAT is assigned the same or different complex refractive indices.[66]

Where α_j are the polarizabilities situated at the position r_j in the lattice arrangement of specific shapes.

The dipole moment is a combination of the external incident field and the fields radiated by all the other dipoles in the array and thus the total electric field as a result of the interaction is given by

$$E_j = E_{inc,j} - \sum_{k \neq j} A_{jk} P_k \tag{7}$$

Here, $E_{inc,j} = E_0 \exp(ik \cdot r_j - i\omega t)$ is the incident electric field, P_k is the polarization, ω is the angular frequency of incident radiation that interacts with the target dipoles, and A_{jk} in the

https://doi.org/10.1021/acsearthspacechem.5c00197
ACS Earth Space Chem. XXXX, XXX, XXX−XXX

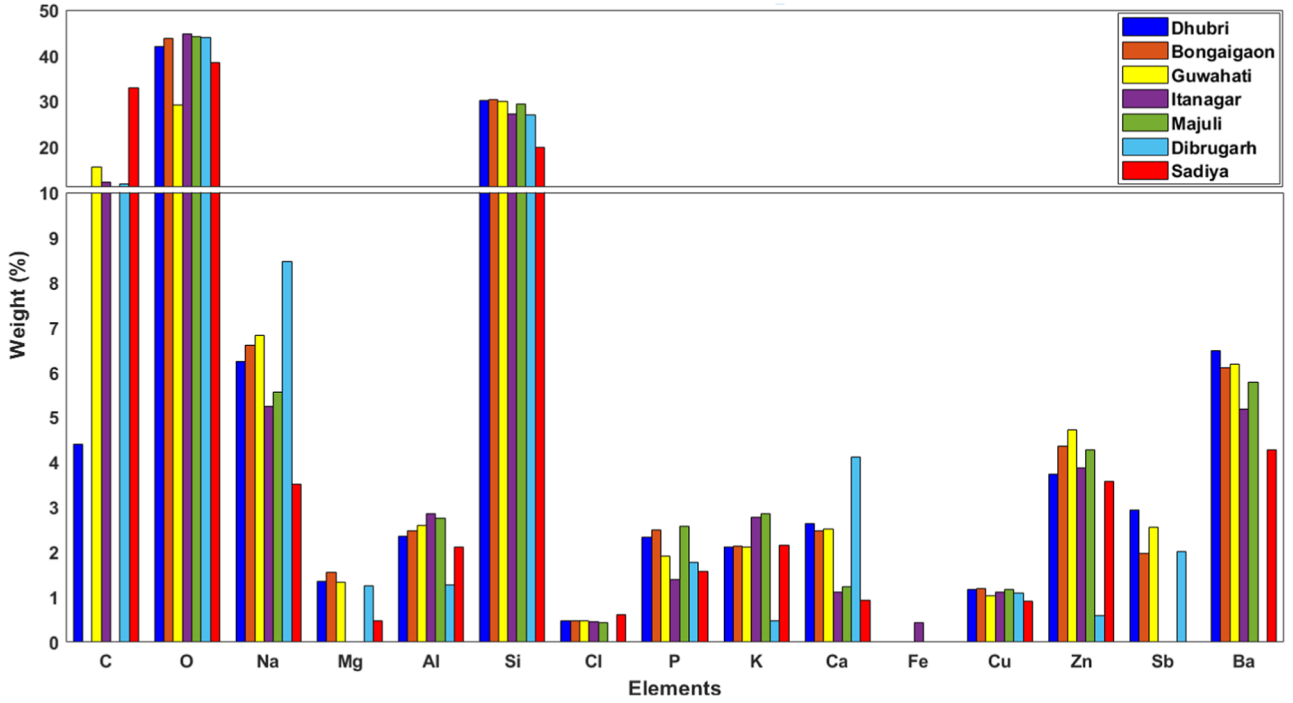

Figure 2. Average weight (%) of different elements in different sectors: western (Dhubri, Bongaigaon, and Guwahati), middle (Itanagar and Majuli), and eastern (Dibrugarh and Sadiya).

interaction equation represents the interaction matrix element given as

$$A_{jk} = \frac{\exp(ikr_{jk})}{r_{jk}}\left[k^2(\hat{r}_{jk}\hat{r}_{jk} - I_3) + \frac{ikr_{jk} - 1}{r_{jk}^{\ 2}}(3\hat{r}_{jk}\hat{r}_{jk} - I_3)\right]_{j\neq k,} \quad (8)$$

where, $r_{jk} = |r_j - r_k|$, $\hat{r}_{jk} = \frac{r_j - r_k}{r_{jk}}$, and I_3 is the identity matrix.

Now, the self-interaction term (interaction of a dipole with itself), i.e. $A_{jj} = \alpha_j^{-1}$, eq 7 becomes

$$E_{inc,j} = \sum_k A_{jk}P_k \quad (9)$$

This process results in an extensive system of linear equations which are solved to find the self-consistent polarization vector for every dipole. Once the dipole moments are known, the DDSCAT code calculates key optical properties such as scattering, absorption, and extinction coefficients, asymmetry parameters for various orientations and polarization states, and Mueller matrix elements.

Thus, the extinction and absorption cross-section can be calculated by solving eq 8 as

$$C_{ext} = \frac{4\pi k}{|E_0|^2}\sum_{j=1}^{N} Im(E_{inc,j}^{*}\cdot P_j) \quad (10)$$

$$C_{abs} = \frac{4\pi k}{|E_0|^2}\sum_{j=1}^{N}\left\{Im[P_j\cdot(\alpha_j^{-1})^{*}P_j^{*}] - \frac{2}{3}k^3|P_j|^2\right\} \quad (11)$$

Here, the * represents the complex conjugate of the respective parameters.

The scattering (Q_{sca}), absorption (Q_{abs}), and extinction (Q_{ext}) efficiencies are calculated as

$$Q_{sca,abs,ext} = C_{sca,abs,ext}/\pi a_{eff}^2 \quad (12)$$

where $C_{sca,abs,ext}$ are scattering, absorption, and extinction optical cross sections, satisfying the following conditions

$$a_{eff} < 9.88\frac{\lambda}{|m|}\left(\frac{N}{10^6}\right)^{1/3} \times or \quad x < \frac{62.04}{|m|}\left(\frac{N}{10^6}\right)^{1/3} \quad (13)$$

When the imaginary part of the refractive index, i.e., Im(m), increases, the DDA solution may overestimate the absorption cross-section C_{abs}. To reduce errors in C_{abs} to acceptable values, interdipole separations d should be smaller than those specified in eq 2.

It is a versatile tool for studying interplanetary dust, atmospheric aerosols, blood cells, marine microbes, and nanostructure arrays. DDA is best suited for particles with moderate size parameters and refractive indices, where accurate modeling of light scattering and absorption by nonspherical or inhomogeneous particles is required. However, it becomes computationally intensive and less precise for very large or highly refractive particles.

3. RESULTS AND DISCUSSION

3.1. Spatial Distribution of Aerosol Chemical Composition. The SEM−EDX analysis reveals the presence of C, O, and Si as the major elements in TSP over all the campaign locations. The wt % of C is overriding in the rural location Sadiya (35%) of the eastern sector, followed by Guwahati (17%), the central city of the western sector. The wt % of O (S) lies within 30−46% (22−32%) in all the locations. The minor elements detected across the region are Na, Mg, Al, P, Cl, Ca, K, Fe, Cu, Zn, Sb, and Ba with wt % < 10%. The highest C content in the rural location Sadiya of the eastern

https://doi.org/10.1021/acsearthspacechem.5c00197
ACS Earth Space Chem. XXXX, XXX, XXX−XXX

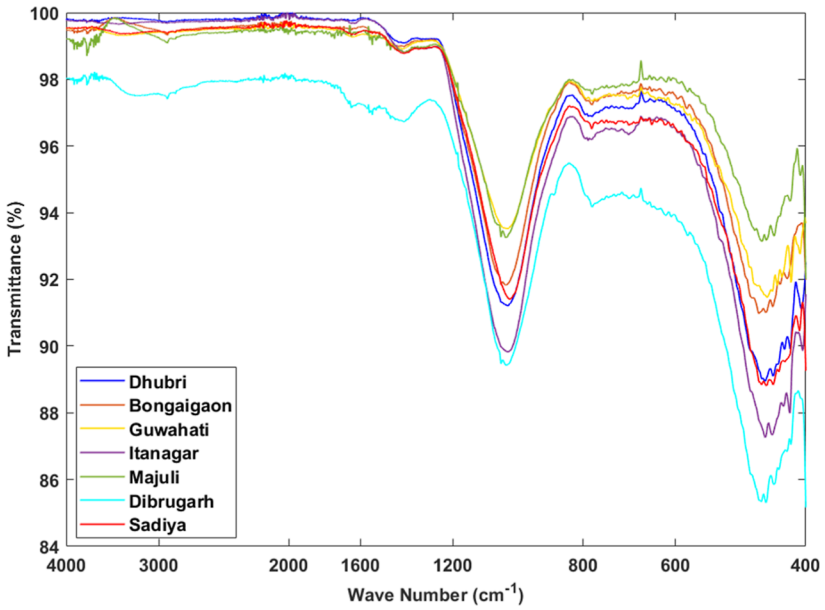

Figure 3. FTIR spectrum of TSP samples collected in different locations over NEI, indicating the presence of quartz, silicate, calcite, aliphatic hydrocarbons, etc.

sector indicates a substantial contribution from sources beyond local anthropogenic ones (Figure 2). The geographical position of this location, encompassed by the Arunachal hills, results in overturning of near-surface wind (Figure 1c), leading to the accumulation and resuspension of aerosols. Being a continental region, the presence of O in TSP is a readily apparent characteristic.[67] Similarly, abundant Si content is also assigned mainly to the continental dust, including local soil dust and remote mineral dust uplifted under fair weather conditions and through long-range transportation, respectively.[68] Na in TSP with wt % lying within 3.8−8.5% is assigned to the sea salt aerosols present over the location,[45] as well as the mineral dust, in terms of wt %, Na is followed by the toxic heavy metals Zn (0.9−4.8%), Cu (1.2−1.4%), and Ba (4.8−7.1%), which can pose a serious threat to the environment and human health. Ba and Zn are released from local or transported industrial smoke, vehicular emissions, agriculture, forestry, biomass burning, mining coal fields and thermal plants, and waste incineration.[69,70] Sb released from both natural and anthropogenic sources, including mining and smelting areas, is found in all locations in the western sector and in the urban area of Dibrugarh in the eastern sector. Fe, the fourth abundant crustal element, is found only in the hilly terrain of Itanagar. The trace elements Al and Ca, which are the third, fourth, and fifth most prevalent elements in the Earth's crust, are also present in the locations with wt % varying between 1.5−3.1 and 1.3−4.2, respectively. Phosphorus (P) (2.1−2.9%) and potassium (K) (0.5−3.1%) primarily originate from natural sources like soil and dust resuspension, sea spray, and biomass burning. Anthropogenic activities, including agriculture, industries, and combustion, also contribute. Majuli Island exhibits the highest P and K concentrations, likely due to its extensive agriculture. Fertile soils, enriched by Brahmaputra River sediments and intensive fertilizer use, contribute significantly to these elevated levels.[71]

Fourier transform infrared (FTIR) spectroscopy is utilized further to characterize TSP to identify its chemical composition and functional groups.[72] This technique detects both organic and inorganic components, such as carbonates, silicates, sulfates, hydrocarbons, and various functional groups, offering insights into pollutant sources, atmospheric transformations, and potential health risks.[73] Quartz, a crystalline silicate mineral with characteristic Si−O vibrational modes at 465 cm^{-1}, 694 cm^{-1}, 777 cm^{-1}, and 1090 cm^{-1}, was found in all analyzed samples.[74,75] Quartz inhalation is linked to respiratory illnesses such as silicosis and lung cancer.[72,76] Other notable components include calcium sulfate at 671 cm^{-1}, nitrate ions (NH_4NO_3) at 713 cm^{-1}, and calcite at 880 cm^{-1}.[77,78] Silicates were identified through Si−O bending at 800 cm^{-1} and CO stretching at 1040 cm^{-1}.[79] Aromatic skeletal stretching and water absorption appeared at 1620 cm^{-1}, while aldehydes and ketones were detected at 1700 cm^{-1}.[77] Organic and elemental carbon were evident at peaks of 671 cm^{-1} and 2111 cm^{-1}, while aliphatic hydrocarbons displayed absorption at 2850 cm^{-1}, 2920 cm^{-1}, 3030 cm^{-1}, and 3400 cm^{-1}[76,78] (Figure 3).

3.2. Morphological Characteristics Based on Elemental Composition. The aerosols have been broadly classified into three categories based on their morphology and elemental composition, a method collectively referred to as single compound spectrum analysis. (i) Biogenic - biologically produced aerosols; (ii) geogenic—derived from soil sediments and weathered rock surfaces; and (iii) anthropogenic—derived from human activities such as industrial, vehicular, and combustion processes (Supporting Information Table S1).

Biogenic (Figure 4a,b), geogenic (Figure 4c,d), and anthropogenic (Figure 4e,f) aerosols exhibit diverse shapes due to their sources and compositions (Table S1). The biogenic aerosols include pollen, fungal spores, and animal or plant debris that have generally distinct morphology, and contain elevated levels of C and O, with critical plant tracers such as Na, Mg, K, P, Si, Fe, Cl, Al, and Ca.[11,15,17,80] The biogenic aerosols are classified by evaluating each bioaerosol using the clustering rule by Coz et al. (2010)[81] based on the constituent elements' weight percentage (C + O) > 75% with 1% of P, K, and Cl < 10%. Geogenic aerosols that are composed chiefly of aluminosilicate, quartz, and calcium particles range from 2 to 80 μm in size and have generally

https://doi.org/10.1021/acsearthspacechem.5c00197
ACS Earth Space Chem. XXXX, XXX, XXX−XXX

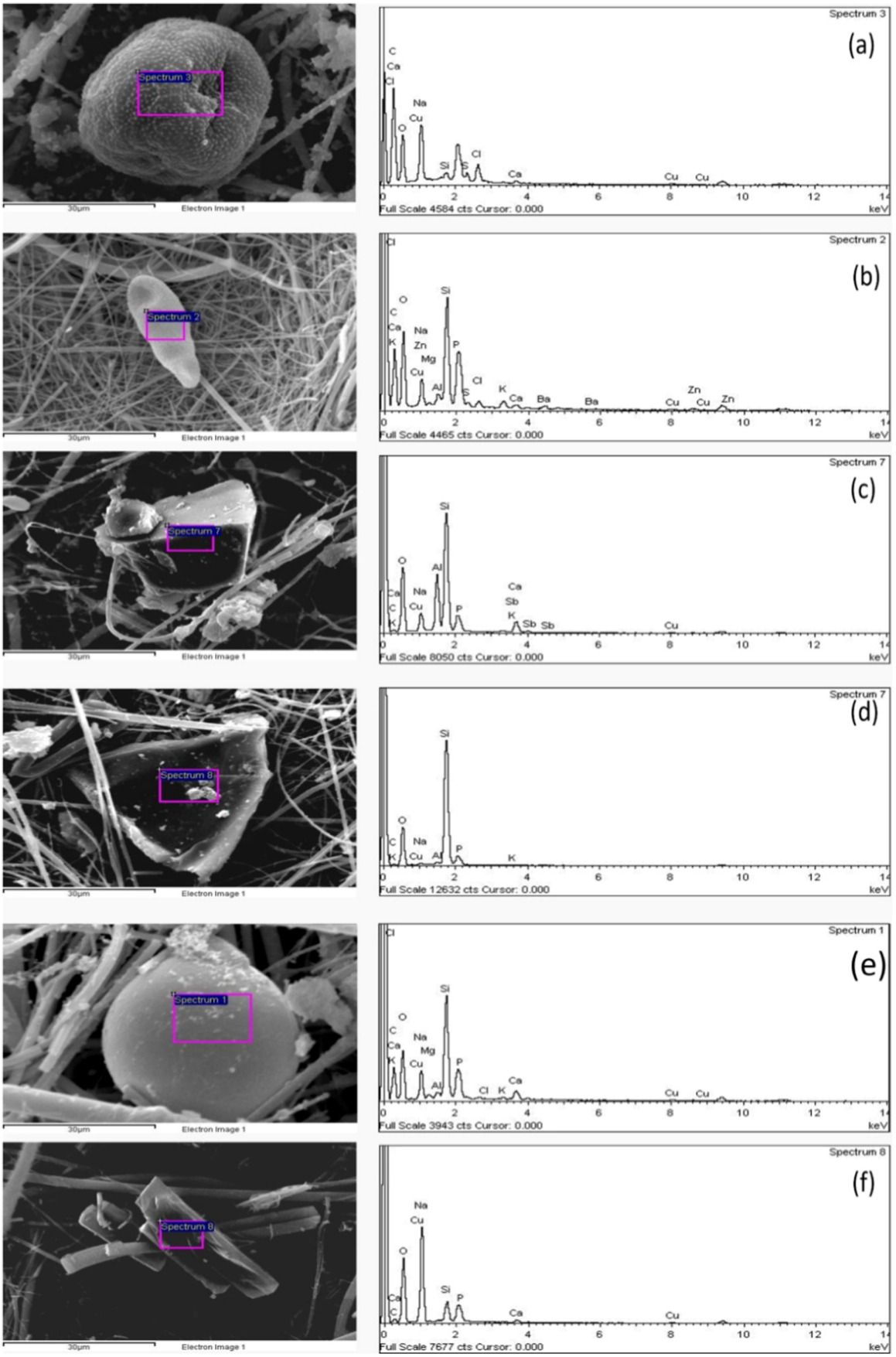

Figure 4. A representative figure of classification of aerosols using single particle spectrum analysis as (a,b) biogenic (c,d) geogenic, and (e,f) anthropogenic aerosols.

https://doi.org/10.1021/acsearthspacechem.5c00197
ACS Earth Space Chem. XXXX, XXX, XXX−XXX

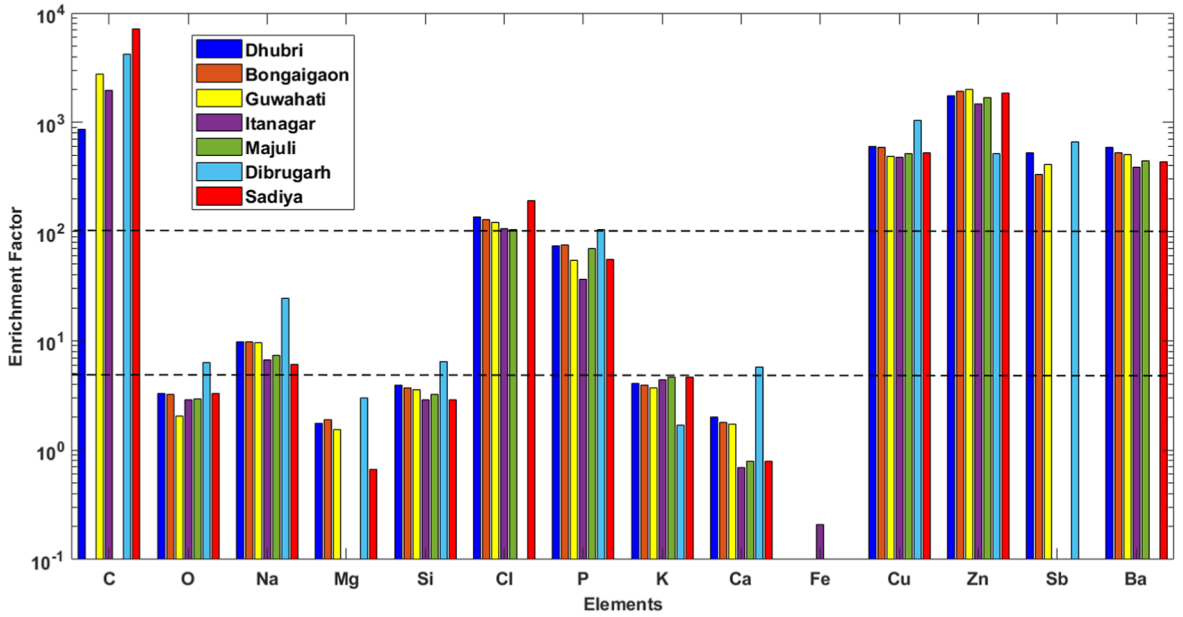

Figure 5. Enrichment factor analysis for different elements at different locations.

rough, irregular, and angular shapes that are typically associated with soil dust and minerals. Around ∼72% of the chemical compounds in the Earth's crust contain elements like Na, Mg, Al, Si, Cl, K, Ca, and Fe.[82,83] Moreover, Chlorine particles that appear within particular areas indicate the influence of agricultural use.[84] Anthropogenic aerosols include iron particles, copper particles, and particles loaded with carbon, which can be spherical, chain-shaped, or indeterminate in shape. A carbon-based aerosol, such as soot, forms branched chain-like particles with primary particles ranging from 30 to 50 nm. Petrol or diesel exhaust produces round particles, whereas natural dust that is suspended produces particles that have well-formed crystalline facet-shaped . Layer-shaped, triangular-shaped, and nearly rectangular-shaped particles also exist, indicating varied non-biogenic sources. Geogenic aerosols have generally defined shapes of crystalline particles, whereas most anthropogenic aerosols are round or amorphous, resulting from industry or combustion processes. The morphological variations of non-biogenic particles make it very complex to group or accurately classify them. This spatial heterogeneity in aerosol composition highlights the influence of local environmental factors and human activity, as well as the growing degree of heterogeneity induced by increasing human influence.[85]

3.3. Source Apportionment. *3.3.1. Enrichment Factor Analysis.* The retrieved chemical composition from SEM−EDX analysis can be further studied to evaluate the anthropogenic impact through source apportionment, i.e., understanding the origin of the chemical species. The estimation of EF using eq 1 is widely applicable, primarily for tracing the anthropogenic contribution of current species. According to Cong et al. (2007),[86] the EF relative to the upper crust composition can be obtained by the expression

$$\mathrm{EF} = ([E]/[R])_{\mathrm{sample}}/([E]/[R])_{\mathrm{crust}} \quad (14)$$

Here, E represents the elemental concentration and R indicates the reference element. Na, Al, Si, Mg, Ca, and Fe are commonly used as reference elements.[87] Aluminum (Al) was chosen as the reference element due to its high crustal abundance, particularly in silicate minerals, and its stability during atmospheric transport. This immobility ensures that Al accurately reflects crustal sources, minimizing the influence of anthropogenic or secondary inputs. enrichment factor (EF) analysis, using Al as a baseline, effectively discriminates between natural geogenic aerosols and other sources, providing valuable insights into aerosol composition and origin at all locations. The EF limits established by Gugamsetty et al. (2012)[88] have been adopted in the present study. Elements with EF <1−5 are considered natural or crustal, primarily derived from dust or soil, while elements with EF ∼5−100 are a mixture of geogenic and anthropogenic origins, and EF >100 are of anthropogenic origin. These are consistent with the work by Duce et al. (1975)[89] and Zoller et al. (1974),[90] who analyzed the elemental composition of aerosols collected from various locations and compared their concentrations to the average composition of the Earth's crust. Lee's (1993)[91] also compiled a list of elemental abundances in the Earth's crust.

The EF values for O, Mg, Si, K, and Ca, and Fe are <1−5, indicating geological origin (soil and dust etc.) (Figure 5). The EF >5 for Na, Cl, and P suggests a mixed origin, influenced by various sources like geogenic, marine, and anthropogenic. Here, Na and Cl are components of marine aerosols, and are also released from geogenic (Na only) and anthropogenic (both Na and Cl) sources like waste incineration and Industrial emissions. In contrast, C, Cu, Zn, Sb, and Ba display EF values greater than 100, signifying a predominantly noncrustal or anthropogenic contribution, often ranging from 100 to 1000 times higher than natural background levels. It demonstrates significant regional variability in elemental contributions across the study sites. Chlorine (Cl) levels are elevated in all areas, indicating a maritime or industrial influence (by trash incineration or chemical operations). However, in a rural area of the middle sector of Majuli, where biogenic contributions dominate, P levels are slightly higher than in other locations, likely due to biological emissions or the use of agricultural fertilizers. Trace metals such as Cu, Zn, and Sb are consistently high in all areas, indicating pervasive anthropogenic emissions from vehicles and industries.

https://doi.org/10.1021/acsearthspacechem.5c00197
ACS Earth Space Chem. XXXX, XXX, XXX−XXX

3.3.2. Principal Component Analysis and Pearson's Correlation Coefficient Analyses. According to the PCA, the two locations in the western sector, Dhubri and Bongaigaon, are dominated by O and Si. Additionally, the metropolitan city of Guwahati exhibits C abundantly in aerosol samples (Table 1). Over Dhubri, Factor 1: O, Si with 98.57% variance

Table 1. Percentage of Total Variance and Possible Sources Obtained for Different Locations of NEI

locations	factor 1	factor 2	factor 3
Dhubri	O, Si	C, Na, Mg, Ca, Cu, Sb	Al, Cl, P, K, Zn, Ba
variance (%)	98.57%	1.17%	0.25%
source	natural (Crustal)	mixed type	mixed type
Bongaigaon	O, Si	Na, Mg, Cl, P, Ca, Sb	Al, K, Cu, Zn, Ba
variance (%)	99.00%	0.98%	0.02%
source	natural (Crustal)	mixed type	mixed type
Guwahati	C, O, Si	Na, P, Ca, K	Al, Cu, Zn, Ba
variance (%)	95.92%	3.72%	0.35%
source	mixed type	crustal	vehicular and industrial
Itanagar	O, Si	C, Ba	Na, Al, Cl, P, K, Ca, Fe, Cu, Zn
variance (%)	98.27%	1.71%	0.007%
source	natural (Crustal)	anthropogenic	mixed type
Majuli	O, Si	Na, Ca, Cu, Ba	Al, Cl, P, K, Zn
variance (%)	99.98%	0.013%	0.004%
source	natural (crustal)	mixed type	mixed type
Dibrugarh	O, Na, Si	Mg, Al, P, K, Ca, Cu, Sb	C, Zn
variance (%)	98.04%	1.92%	0.04%
source	natural (crustal)	mixed type	industrial and vehicular
Sadiya	C, O, Si	Na, Al, Cl, P, K, Cu, Zn, Ba	Mg, Ca
variance (%)	84.80%	15.15%	0.03%
source	anthropogenic	mixed	crustal

indicates a strong crustal source, also consistent with EF results that assign a large amount of the aerosol composition to soil dust and mineral components. Factor 2 (C, Na, Mg, Ca, Cu, and Sb; 1.17%) indicates a mixture of natural and anthropogenic sources, including transportation and industrial emissions. This is consistent with the EF analysis suggesting a high enrichment of elements like Cu and Sb due to industrial emissions and traffic pollution. Factor 3 (Al, Cl, P, K, Zn, Ba; 0.25%) emphasizes the influence of anthropogenic sources such as industrial emissions, vehicle exhaust, and possibly agricultural activities. This is consistent with the PCC study, where Al exhibits a strong correlation with Ba, Zn, Cu, K, and P. Also, P and K strongly correlate with Ba, Zn, and Cu, and Mg with Sb and Ca (Figure 6c). The correlation of Sb with Mg, Si, and Ca indicates that TSP originated from traffic pollution, industrial activity, and building dust.[92,93] Further, Ba coexists with Al, P, K, Zn, and Cu in the urban environments of Guwahati and Dhubri, supporting contributions from automotive emissions and industrial operations.[94] In Bongaigaon Factor 1 (O, Si; 99.00% variance), the dominance of natural sources, particularly mineral dust and soil resuspension, is highlighted. Factor 2 (Na, Mg, Cl, P, Ca, Sb; 0.98%) indicates mixed sources, including marine and anthropogenic sources, such as agricultural activities, as also evident from the EF analysis. This is also evidenced by the existing strong correlation among Na, Ca, Si, Mg, and K, Cu, Zn, and Ba (Figure 6d). PCC results, showing a strong correlation of O with Na, Mg, Si, and Ca, demonstrate the prevalence of oxides of these elements in the continental atmosphere. The minor anthropogenic factor, Factor 3 (Al, K, Cu, Zn, and Ba; 0.02%), is associated with industrial and vehicular emissions. This is also supported by Pearson's correlation, of Al with Ba, Zn, Cu; Si with Na, Mg, O; Ca with Na, Mg, Si, O. The correlation between Ca, Na, Mg, and Si represents natural sources like soil dust, marine aerosols, and construction activities,[95] with the Ca−Si relationship specifically linked to soil weathering and resuspension.[94] In Guwahati, the third location in the western sector and the only metropolitan city of the region, Factor 1 (C, O, Si; 95.92%) variance suggests a combination of crustal sources and biomass burning, as also indicated by both the EF and PCC analyses, with a strong correlation between Si and C (Figure 6b). The high correlation of C and Si in Pearson's analysis further supports this finding, pointing to a mix of natural and anthropogenic sources. Factor 2, dominated by Na, P, Ca, and K (3.72%), reflects crustal material, in line with the EF results. Moreover, PCC shows that Na and Ca are highly correlated. The anthropogenic influence is confirmed in Factor 3 (Al, Cu, Zn, Ba; 0.35%), where strong correlations among Al, Ba, Zn, and K in Pearson's analysis point toward common sources like vehicular emissions and industrial activities. The significant correlation of Al with K, Zn, and Ba suggests soil resuspension and metal-containing urban dust from a variety of sources, including traffic emissions, industrial activity, and building.[92]

In the middle sector location, Itanagar, the Factor 1 (O, Si; 98.27%) corresponds to natural crustal inputs from soil erosion and resuspension, but Factor 2 (C, Ba; 1.71%) suggests a mixture of natural and anthropogenic sources, mainly soil erosion and biomass burning, which is also indicated from EF analysis. Factor 3 (Na, Al, Cl, P, K, Ca, Fe, Cu, Zn; 0.007%) means the anthropogenic influence from industrial, vehicular, and construction activities. These are also supported by strong Pearson's correlation among Na, Al, Si, K, Ba, Zn, and Cu, indicating their shared anthropogenic origin. The oxides of Si, P, Cu, and Zn are also evident from their strong correlation with O. In the river island Majuli, Factor 1 (O, Si; 99.98%) represents natural crustal sources, similar to other locations. However, Factor 2 (Na, Ca, Cu, Ba; 0.013%) is more closely related to mixed sources, including agricultural activities, combustion, and soil corrosion. The minimal industrial influence is evident from Factor 3 (Al, Cl, P, K, Zn; 0.004%). These observations are also supported by the existing strong Pearson's correlation between P and Ba, K and Zn, Cu and Na, Si and Ca, indicating emission of the species from local agricultural activities and biomass combustion.

In the urban location Dibrugarh of the eastern sector, Factor 1, dominated by O, Na, and Si (98.04% variance), indicates aerosols originating from natural, crustal sources, including soil and mineral dust. This is consistent with the EF analysis, demonstrating the majority of the elements of geogenic origin. The Factor 2, reflecting mixed sources with abundant elements like Mg, Al, P, K, Ca, Cu, and Sb (1.92% variance) is consistent with the human contributions (e.g., agricultural operations and local industries) revealed by the EF analysis and the PCC results with significant correlation of Ca with Mg, Al and Si; Cu with Mg and P; Na and K; Sb and O (Figure 6a). The

https://doi.org/10.1021/acsearthspacechem.5c00197
ACS Earth Space Chem. XXXX, XXX, XXX−XXX

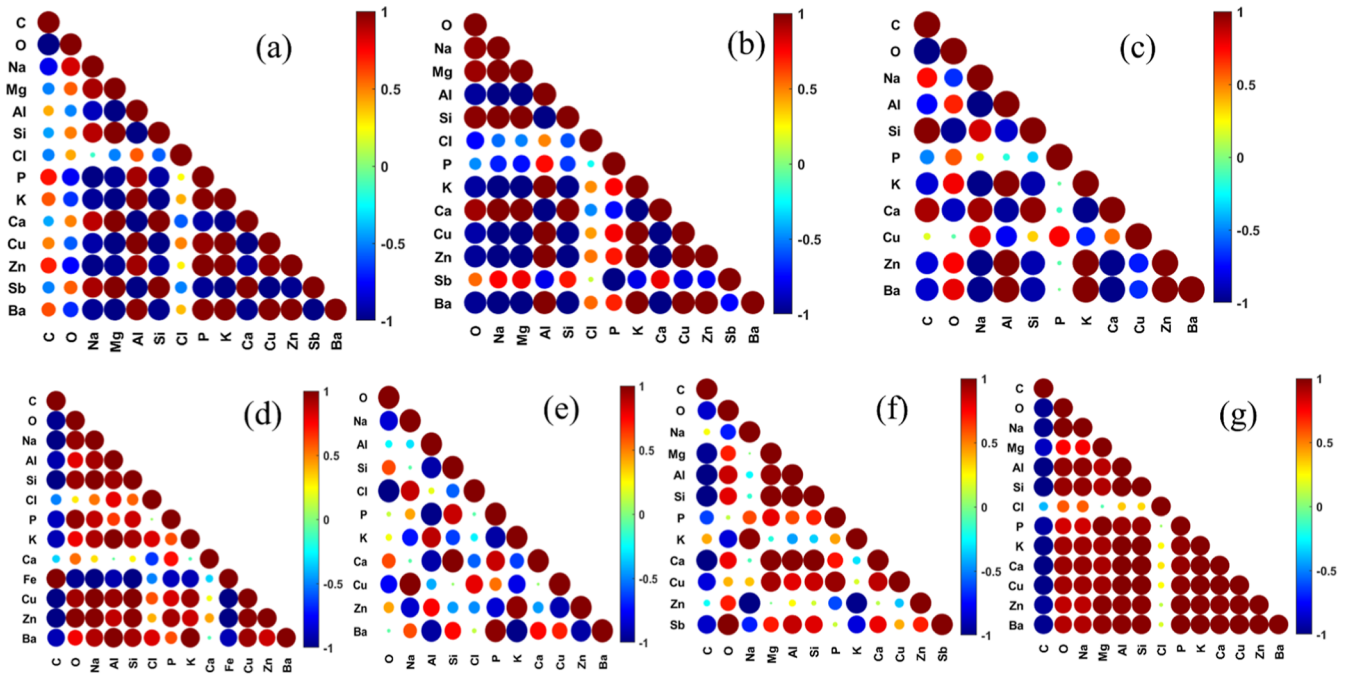

Figure 6. PCC analysis for different elements over the eastern sector (a−c Dhubri, Bongaigaon, Guwahati), the Middle sector (d,e Itanagar and Majuli), and the eastern sector (f,g Dibrugarh, and Sadiya). The color bar and size of the circles indicate the correlation coefficient among different elements. The correlation matrices obtained from Pearson's correlation coefficient analysis demonstrate the association of different elements released from common sources.

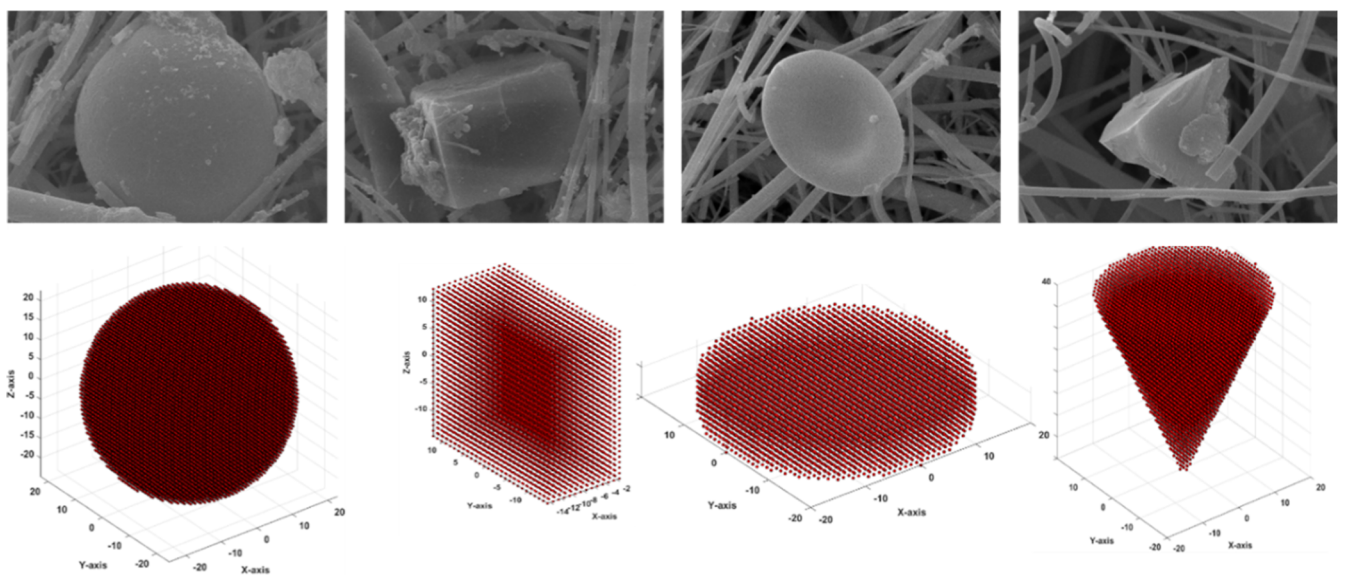

Figure 7. Dust aerosols of different shapes: spherical, rectangular, disc, and cone (top panel) observed over the sampled locations during the campaign. The same shapes are considered for DDSCAT simulations for the optical properties (bottom panel).

factor 3 (C, Zn) with negligible variance (0.04%) suggests anthropogenic emissions, especially related to industrial and vehicular activities. Ca is strongly associated with Mg, Al, and Si, which can be assigned to the clay minerals and feldspars, and soil resuspension.[96] In Sadiya, a major rural location in the eastern sector, Factor 1 (C, O, Si; 84.80%) implies a combination of natural crustal sources and carbonaceous materials, originating primarily from biomass burning. Further, factor 2 (Na, Al, Cl, P, K, Cu, Zn, Ba; 15.15%) represents emissions from a variety of sources, including agriculture, industry, and vehicles. Cu and Zn likely stem from agricultural practices involving fertilizers and pesticides, while Ba and P emissions are associated with the burning of plant debris.[97] Further, P, Ca, K, Cu, Zn, and Ba appear to have common origins such as agricultural processes, building, and industrial emissions. The significant connection of Al and Si with these elements in Sadiya further supports the presence of mixed sources, including both natural and anthropogenic emissions. Factor 3 (Mg, Ca; 0.03%) (Table 1) again indicates natural sources like soil erosion and resuspensions, most likely due to the dried sandy river Brahmaputra.

3.4. Estimation of Optical Properties of Dust Aerosols Using DDSCAT. According to the source apportionment analyses discussed in a previous section, all selected locations

https://doi.org/10.1021/acsearthspacechem.5c00197
ACS Earth Space Chem. XXXX, XXX, XXX−XXX

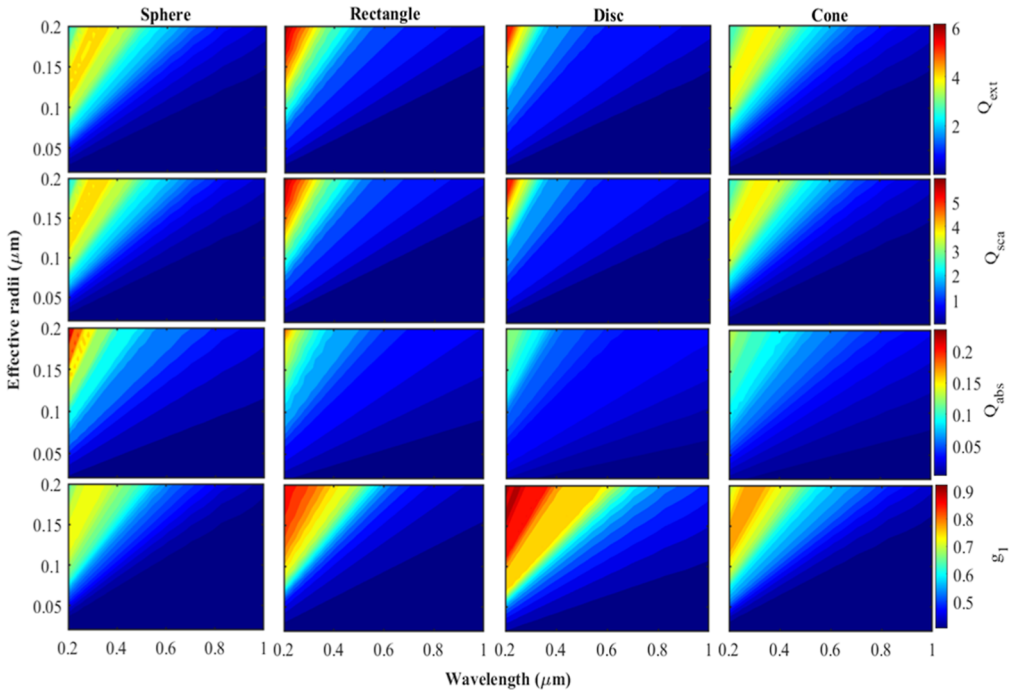

Figure 8. DDSCAT simulated spectral variation of aerosol optical properties: Extinction, scattering, absorption, and asymmetric parameter, for different shapes: sphere, rectangle, disc, and cone, and sizes represented by effective radius (0.02−0.2 μm), within the wavelength range 0.2 μm−1 μm.

are primarily influenced by dust aerosols, which contain mainly Si and O. Therefore, dust aerosols have been considered for simulating optical properties using DDSCAT for different shapes obtained from SEM−EDX analysis. The real shapes—spherical, rectangular, disc, and cone—of dust aerosols (Figure 7, top panel) are used to match the designed dipole arrays of irregular shapes (Figure 7, bottom panel) for DDSCAT simulation, as discussed in Section 2.5. The effective radius of the dipole array is considered within the range 0.02−0.2 μm to satisfy eq 14, where the dipole separation (d) lies within (1.6−16) × 10^{-3} μm, provided the condition in eq 2 is satisfied. This allows us to consider the wavelength (λ) range from ultraviolet (UV) to infrared (IR) for interactions with dust aerosols of different shapes and sizes. We are considering the complex refractive index (m) of dust aerosols for the present simulation as m = 1.53 + 0.0078i.[98] The complex refractive index, an intrinsic optical property, is dependent on wavelength and aerosol composition and influences the scattering and absorption efficiencies.[99] Further, different aerosol constituents interact differently with radiation across the solar spectrum, thereby resulting in spectral variation in aerosol radiative effects.[100] Moreover, the aerosols of various sizes and nonspherical or irregular shapes, such as dust, can alter scattering angles and absorption or scattering compared to spheres, affecting the key optical parameters like aerosol optical depth, phase functions, and single scattering albedo,[102] which are crucial for assessing aerosol−climate interaction assessed through radiative forcing estimations. Thus, DDSCAT simulations were performed by considering variations in both the particle shape and size of dust aerosols across the wavelength range of 0.02−0.2 μm, as mentioned. above (see Table 1).

The shape of the particles exhibits a noticeable impact on the optical properties (Figure 8; Table 2). The aerosols of rectangular shapes exhibit maximum extinction (up to Q_{ext} = 6.18) and scattering (up to Q_{sca} = 6.01) efficiencies, along with asymmetry parameter (up to g = 0.88), followed by discs and spheres (Table 2). This implies that nonspherical aerosols are more efficient in attenuating light in the atmosphere. Absorption efficiency is relatively low for all the shapes, indicating dominance of scattering in the extinction process. It is higher for spherical dust particles (up to Q_{abs} = 0.23), followed by a rectangular shape, at lower wavelengths. This suggests that spherical particles, due to their symmetry, may have small resonant benefits at shorter wavelengths, which are less noticeable in nonspherical particles, presumably due to scattering fluctuations and angle-dependent resonance in irregular shapes.[101] All efficiencies increase with increasing effective radii for all shapes due to their available higher surface area and volume, allowing for more interaction with incident light.

Table 2. The Maximum Values of all the Three Efficiencies and the Asymmetry Parameter for Different Shapes of Dust Aerosols Simulated Using DDSCAT

shape	Q_ext	Q_sca	Q_abs	g
sphere	4.25	4.02	0.23	0.60
rectangle	6.18	6.02	0.16	0.88
disc	5.60	5.46	0.14	0.91
cone	4.10	3.96	0.14	0.71

The wavelength and size dependence of the optical properties are further investigated by fixing the effective radius at ∼ 0.2 μm and the wavelength at 0.55 nm, respectively (Figures 9 and 10). The spectral variation of the extinction and scattering efficiencies for spherical and cone-shaped aerosols behaves differently from that of the rectangular and disc-shaped aerosols (Figure 9). The rectangular shape exhibits the highest extinction efficiency, followed by the disc at shorter wavelengths (0.2−0.3 μm). The sphere and cone initially

https://doi.org/10.1021/acsearthspacechem.5c00197
ACS Earth Space Chem. XXXX, XXX, XXX−XXX

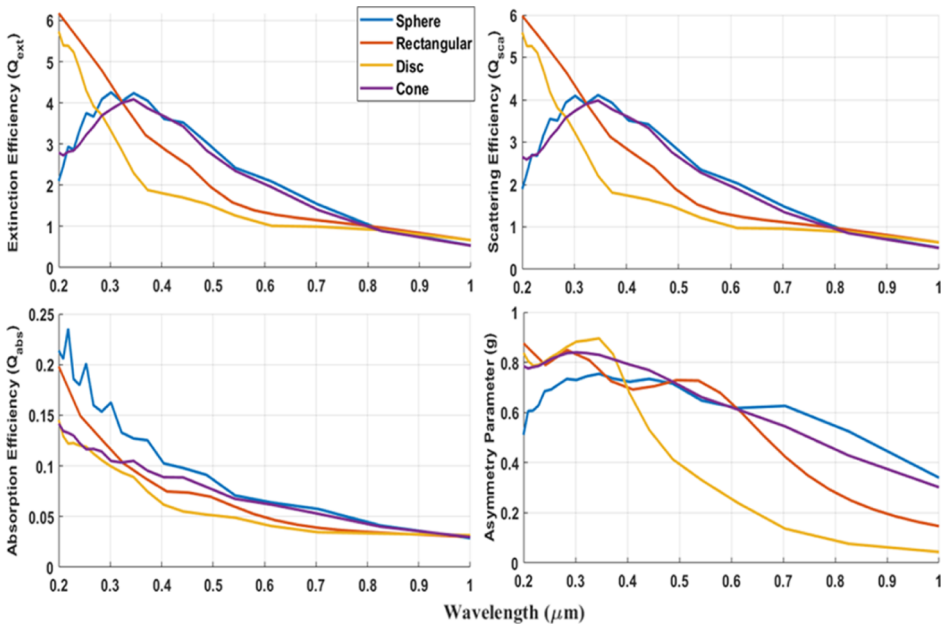

Figure 9. DDSCAT simulated spectral variation of aerosol optical properties: extinction, scattering, absorption, and asymmetric parameter, for different shapes: sphere, rectangle, disc, and cone, at fixed size with effective radius 0.2 μm within the wavelength range 0.2 μm−1 μm.

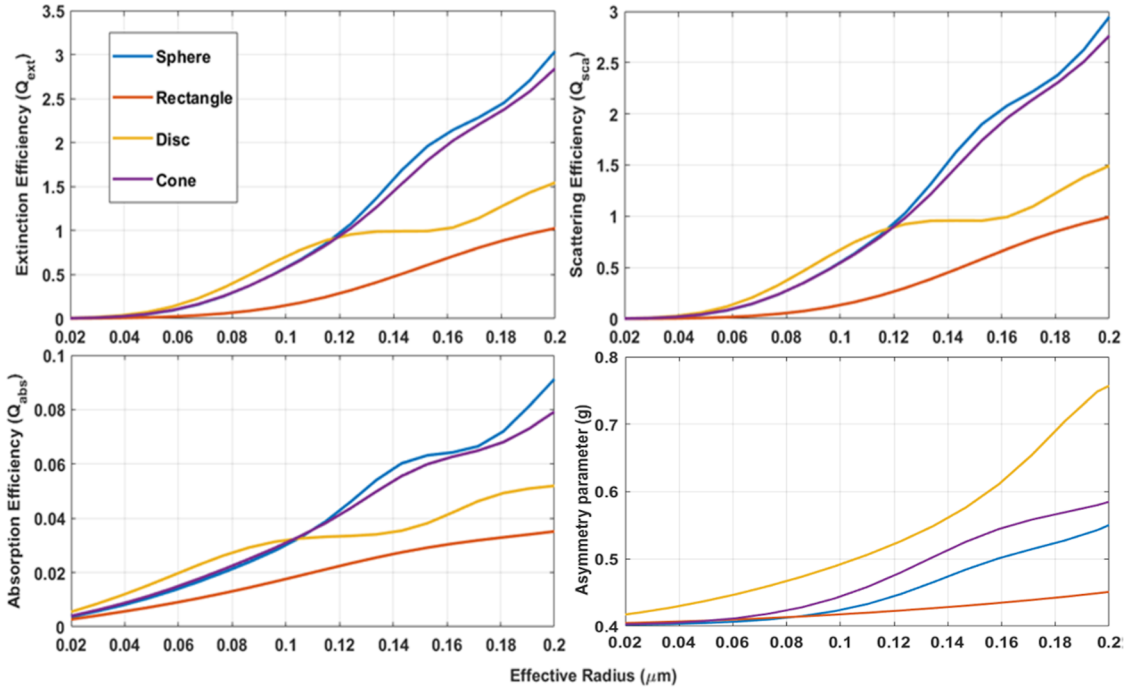

Figure 10. DDSCAT simulated spectral variation of aerosol optical properties includes extinction, scattering, absorption, and the asymmetric parameter for different shapes: sphere, rectangle, disc, and cone having size represented by effective radius range 0.02−0.2 μm at a specific wavelength (0.55 μm).

increase from 0.2 to 0.35 μm, then gradually decrease, tending to converge at IR (>0.76 μm). The rectangle and disc-shaped particles have substantially larger surface area than spherical particles, resulting in a more intense interaction with electromagnetic radiation. In contrast, the absorption efficiency is maximum for the spheres (Q_{abs} = 0.24 at λ = 0.2 μm), followed by rectangular-shaped aerosols. At λ ∼0.2 μm, spherical type of dust aerosols generally exhibit increased absorption compared to longer wavelengths due to the presence of iron oxides, such as hematite and goethite, in mineral dust, which show strong absorption in the UV and near-UV spectrum.[102] However, at λ ∼0.55 μm, all the efficiencies maximize for discs at a_{eff} < 0.12 μm, but beyond that, the spherical shape takes precedence, followed by the cone. Q_{ext} and Q_{sca} increase consistently with an increase in effective radius for a_{eff} < 0.12 μm for the spheres and cones, following the Mie theory and realistic atmospheric particle morphologies, where rotational symmetry and curvature facilitate stronger light−particle interactions.[103] Q_{abs} also exhibit a similar pattern.

https://doi.org/10.1021/acsearthspacechem.5c00197
ACS Earth Space Chem. XXXX, XXX, XXX−XXX

The disc (up to $g = 0.91$) and rectangular-shaped aerosols (up to $g = 0.88$) show more pronounced forward scattering, meaning that these would affect light transmission through the atmosphere differently than the spherical aerosols.[28] This has implications for remote sensing and satellite observations, where forward-scattering is crucial. For a fixed effective radius, all the shapes exhibit the highest asymmetry parameter at shorter wavelengths (0.2−0.4 μm), indicating significant forward scattering (Figure 9). The forward scattering increases with increasing a_{eff} for all shapes of aerosols at a fixed $\lambda \sim 0.55$ μm (Figure 10). The disc and cone-shaped aerosols are efficient forward scatterers.

4. CONCLUSIONS

The chemical composition of aerosols is the most critical factor for their complex roles in both climate change and pollution control. Different chemical species have distinct radiative and toxic properties, necessitating their characterization from as many locations as possible. Hence, an attempt has been made for the first time to characterize regional aerosols by collecting TSP samples using a High-Volume Sampler from seven distinct locations in NEI. The EDX and SEM analyses of these samples identified C, O, and Si as the major contributors to atmospheric aerosols in the region, with the eastern sector more dominant in C content. Similar FTIR spectra have been observed across the region containing calcite, silicate, pyroskite, Illite, and aliphatic hydrocarbons. Based on single-particle spectrum analysis, the particles were categorized into biogenic, geogenic, and anthropogenic categories. The integrated source apportionment study, employing Enrichment Factor analysis, Principal Component Analysis, and Pearson Correlation Coefficient, reveals that natural sources, primarily containing soil and mineral dust, dominate in most of the locations. At the same time, trace metals like Cu, Zn, Ba, and Sb indicate significant anthropogenic contributions mainly from industrial emissions, vehicle activity, and agricultural operations. The mixed nature of some places emphasizes the interaction of natural and anthropogenic sources over the region. This type of study, which includes information on aerosol chemical components and source identification, is essential for effective, target-oriented pollution control and climate change mitigation measures. Thus, the present study directly advances Climate Action-the Sustainable Development Goal 13.

The chemical composition of aerosols is integral to determining the refractive index of the particles. The refractive index and the morphology of aerosol particles are crucial for accurately simulating optical and radiative properties. The nonspherical or irregular mineral dust particles scatter more light in the forward direction and thus decrease backscattering and hence lessen the net cooling effect relative to a spherical assumption.[104] This can result in greater diffuse radiation at the surface and more atmospheric heating aloft, impacting regional energy balance and cloud processes. Thus, the distinct shapes of dust aerosols obtained from SEM analysis are further used to simulate the optical properties using DDSCAT. The extinction and scattering efficiencies hence obtained are in the order of magnitude for rectangular > disc > cone > sphere. The disc and cone-shaped dust aerosols are found to exhibit more positive asymmetry and behave as efficient forward scatterers compared to spherical and rectangular, with the overall asymmetry parameter increasing with size for all shapes. This information is essential for reducing uncertainty in radiative transfer calculations, understanding the aerosol−climate interaction, and for remote sensing applications. Overall, the present study has added to the existing knowledge of regional aerosol properties, including spatiotemporal heterogeneity and aerosol−radiation interactions. However, long-term observations to investigate seasonality in aerosol chemical composition and source variability across different locations, including additional analytical techniques.

■ ASSOCIATED CONTENT

Supporting Information

The Supporting Information is available free of charge at https://pubs.acs.org/doi/10.1021/acsearthspacechem.5c00197.

Table S1: Classification of compounds into different groups: (biogenic, geogenic, and anthropogenic) using SEM−EDX single compound spectrum analysis on PM samples over different locations of NEI (PDF)

■ AUTHOR INFORMATION

Corresponding Author

Binita Pathak − *Department of Physics, Dibrugarh University, Dibrugarh, Assam 786004, India; Centre for Atmospheric Studies, Dibrugarh University, Dibrugarh, Assam 786004, India;* orcid.org/0000-0002-8314-6819; Email: binita@dibru.ac.in

Authors

Barlin Das − *Department of Physics, Dibrugarh University, Dibrugarh, Assam 786004, India; Jorhat Institute of Science and Technology, Jorhat, Assam 785010, India*

Partha Jyoti Sahu − *Department of Physics, Dibrugarh University, Dibrugarh, Assam 786004, India*

Mukunda Madhab Gogoi − *Space Physics Laboratory, Vikram Sarabhai Space Centre, Thiruvananthapuram 695022, India*

Pradip Kumar Bhuyan − *Centre for Atmospheric Studies, Dibrugarh University, Dibrugarh, Assam 786004, India*

Krishnanka Jyoti Baishya − *Centre for Atmospheric Studies, Dibrugarh University, Dibrugarh, Assam 786004, India*

Pranami Mahanta − *Centre for Atmospheric Studies, Dibrugarh University, Dibrugarh, Assam 786004, India*

Kalyan Bhuyan − *Department of Physics, Dibrugarh University, Dibrugarh, Assam 786004, India; Centre for Atmospheric Studies, Dibrugarh University, Dibrugarh, Assam 786004, India*

Jhuma Biswas − *Department of Physics, Pandu College, Guwahati, Assam 781012, India*

Rumajyoti Hazarika − *Department of Physics, Jengraimukh College, Majuli, Assam 785105, India*

Saradi Bora − *Department of Physics, Sadiya College, Sadiya, Assam 786157, India*

Malabika Borah − *Department of Chemistry, B. N. College (Autonomous), Dhubri, Assam 783324, India*

Romesh Borgohain − *Department of Chemistry, Birjhora Mahavidyalaya, Bongaigaon, Assam 783380, India*

Jagannath Bhuyan − *Department of Chemistry, NERIST, Nirjuli, Arunachal Pradesh 791112, India*

Kakali Bhuyan − *North Lakhimpur University, North Lakhimpur, Assam 787031, India*

Swapnali Hazarika − *CSIR-North East Institute of Science & Technology, Jorhat, Assam 785006, India*

https://doi.org/10.1021/acsearthspacechem.5c00197
ACS Earth Space Chem. XXXX, XXX, XXX−XXX

Complete contact information is available at:
https://pubs.acs.org/10.1021/acsearthspacechem.5c00197

Notes

The authors declare no competing financial interest.

■ ACKNOWLEDGMENTS

The work is a major goal of the Aerosol Radiative Forcing over India (ARFI) project, ongoing at Dibrugarh University under the ISRO-GBP. P.J.S. and K.J.B. are thankful to ISRO GBP ARFI for providing fellowships. B.D. is grateful to SERB, Department of Science and Technology, Govt. of India, for providing the fellowship under the WEA Project: WEA/2021/000013. J.B. is indebted to the Indian Academy of Sciences for a summer research fellowship. J.B. also acknowledges the DST, Anusandhan National Research Foundation, New Delhi, for financial support under the project File No. EEQ/2023/001120. The authors acknowledge the ANRF PURSE Project ongoing at Dibrugarh University.

■ REFERENCES

(1) Intergovernmental Panel On Climate Change (IPCC). *Climate Change 2021—the Physical Science Basis: Working Group I Contribution to the Sixth Assessment Report of the Intergovernmental Panel on Climate Change*, 1st ed.; Cambridge University Press, 2023.

(2) Agrawal, A.; Upadhyay, V. K.; Sachdeva, K. Study of Aerosol Behavior on the Basis of Morphological Characteristics during Festival Events in India. *Atmos. Environ.* **2011**, *45* (21), 3640−3644.

(3) Pipal, A. S.; Kulshrestha, A.; Taneja, A. Characterization and Morphological Analysis of Airborne PM2.5 and PM10 in Agra Located in North Central India. *Atmos. Environ.* **2011**, *45* (21), 3621−3630.

(4) Salma, I.; Maenhaut, W.; Zemplén-Papp, E. ·; Záray, G. Comprehensive Characterisation of Atmospheric Aerosols in Budapest, Hungary: Physicochemical Properties of Inorganic Species. *Atmos. Environ.* **2001**, *35* (25), 4367−4378.

(5) Kaur, P.; Rahaman, M.; Guha, A. Elemental Characterization and Morphological Analysis of Atmospheric Aerosols in a Rural-Continental Environment of Northeast India. *Arab. J. Geosci.* **2022**, *15* (24), 1752.

(6) Misra, A.; Gaur, A.; Bhattu, D.; Ghosh, S.; Dwivedi, A. K.; Dalai, R.; Paul, D.; Gupta, T.; Tare, V.; Mishra, S. K.; Singh, S.; Tripathi, S. N. An Overview of the Physico-Chemical Characteristics of Dust at Kanpur in the Central Indo-Gangetic Basin. *Atmos. Environ.* **2014**, *97*, 386−396.

(7) Zhang, D.; Ishizaka, Y.; Aryal, D. Individual Particles and Droplets in Continentally Influenced Stratocumulus: A Case Study over the Sea of Japan. *Atmospheric Res.* **2006**, *79* (1), 30−51.

(8) Li, W.; Shao, L. Transmission Electron Microscopy Study of Aerosol Particles from the Brown Hazes in Northern China. *J. Geophys. Res. Atmospheres* **2009**, *114* (D9), 2008JD011285.

(9) Pósfai, M.; Buseck, P. R. Nature and Climate Effects of Individual Tropospheric Aerosol Particles. *Annu. Rev. Earth Planet. Sci.* **2010**, *38* (1), 17−43.

(10) Hu, T.; Cao, J.; Shen, Z.; Wang, G.; Lee, S.; Ho, K. Size Differentiation of Individual Atmospheric Aerosol during Winter in Xi'an, China. *Aerosol Air Qual. Res.* **2012**, *12* (5), 951−960.

(11) Kaur, P.; Rahaman, M.; Guha, A. Elemental Characterization and Morphological Analysis of Atmospheric Aerosols in a Rural-Continental Environment of Northeast India. *Arab. J. Geosci.* **2022**, *15* (24), 1752.

(12) Deka, P.; Hoque, R. R. Incremental Effect of Festive Biomass Burning on Wintertime PM10 in Brahmaputra Valley of Northeast India. *Atmospheric Res.* **2014**, *143*, 380−391.

(13) Pandey, A.; Venkataraman, C. Estimating Emissions from the Indian Transport Sector with On-Road Fleet Composition and Traffic Volume. *Atmos. Environ.* **2014**, *98*, 123−133.

(14) Srivastava, A.; Gupta, S.; Jain, V. K. Winter-Time Size Distribution and Source Apportionment of Total Suspended Particulate Matter and Associated Metals in Delhi. *Atmospheric Res.* **2009**, *92* (1), 88−99.

(15) Pachauri, T.; Singla, V.; Satsangi, A.; Lakhani, A.; Kumari, K. M. SEM-EDX Characterization of Individual Coarse Particles in Agra, India. *Aerosol Air Qual. Res.* **2013**, *13* (2), 523−536.

(16) Gogoi, M. M.; Thakur, R. C.; Gazi, S.; Nair, V. S.; Mohan, R.; Babu, S. S. Vertical Distributions of the Microscopic Morphological Characteristics and Elemental Composition of Aerosols over India. *J. Atmospheric Chem.* **2020**, *77* (4), 117−140.

(17) Panda, U.; Boopathy, R.; Gadhavi, H. S.; Renuka, K.; Gunthe, S. S.; Das, T. Metals in Coarse Ambient Aerosol as Markers for Source Apportionment and Their Health Risk Assessment over an Eastern Coastal Urban Atmosphere in India. *Environ. Monit. Assess.* **2021**, *193* (5), 311.

(18) Adachi, K.; Chung, S. H.; Buseck, P. R. Shapes of Soot Aerosol Particles and Implications for Their Effects on Climate. *J. Geophys. Res. Atmospheres* **2010**, *115* (D15), 2009JD012868.

(19) Vione, D.; Maurino, V.; Minero, C.; Pelizzetti, E.; Harrison, M. A. J.; Olariu, R.-I.; Arsene, C. Photochemical Reactions in the Tropospheric Aqueous Phase and on Particulate Matter. *Chem. Soc. Rev.* **2006**, *10*, 1039.b510796m.

(20) Ghio, A. J.; Devlin, R. B. Inflammatory Lung Injury after Bronchial Instillation of Air Pollution Particles. *Am. J. Respir. Crit. Care Med.* **2001**, *164* (4), 704−708.

(21) Li, L.; Wang, W.; Feng, J.; Zhang, D.; Li, H.; Gu, Z.; Wang, B.; Sheng, G.; Fu, J. Composition, Source, Mass Closure of PM2.5 Aerosols for Four Forests in Eastern China. *J. Environ. Sci.* **2010**, *22* (3), 405−412.

(22) Jacobson, M. Z. *Fundamentals of Atmospheric Modeling*, 2nd ed.; Cambridge University Press, 2005.

(23) Mishchenko, M. I.; Travis, L. D.; Lacis, A. A. *Scattering, Absorption, and Emission of Light by Small Particles*; Cambridge University Press, 2002; Vol. *4*.

(24) Legrand, M.; Dubovik, O.; Lapyonok, T.; Derimian, Y. Accounting for Particle Non-Sphericity in Modeling of Mineral Dust Radiative Properties in the Thermal Infrared. *J. Quant. Spectrosc. Radiat. Transfer* **2014**, *149*, 219−240.

(25) Herrera, M. E.; Dubovik, O.; Torres, B.; Lapyonok, T.; Fuertes, D.; Lopatin, A.; Litvinov, P.; Chen, C.; Benavent-Oltra, J. A.; Bali, J. L.; Ristori, P. R. Estimates of Remote Sensing Retrieval Errors by the GRASP Algorithm: Application to Ground-Based Observations, Concept and Validation. *Atmospheric Meas. Technol.* **2022**, *15* (20), 6075−6126.

(26) Mishchenko, M. I.; Geogdzhayev, I. V.; Cairns, B.; Rossow, W. B.; Lacis, A. A. Aerosol Retrievals over the Ocean by Use of Channels 1 and 2 AVHRR Data: Sensitivity Analysis and Preliminary Results. *Appl. Opt.* **1999**, *38* (36), 7325.

(27) Mishchenko, M. I.; Geogdzhayev, I. V.; Cairns, B.; Rossow, W. B.; Lacis, A. A. Aerosol Retrievals over the Ocean by Use of Channels 1 and 2 AVHRR Data: Sensitivity Analysis and Preliminary Results. *Appl. Opt.* **1999**, *38* (36), 7325.

(28) Mishchenko, M. I.; Travis, L. D.; Kahn, R. A.; West, R. A. Modeling Phase Functions for Dustlike Tropospheric Aerosols Using a Shape Mixture of Randomly Oriented Polydisperse Spheroids. *J. Geophys. Res. Atmospheres* **1997**, *102* (D14), 16831−16847.

(29) Kahnert, M. Electromagnetic Scattering by Nonspherical Particles: Recent Advances. *J. Quant. Spectrosc. Radiat. Transfer* **2010**, *111* (11), 1788−1790.

(30) Dubovik, O.; Holben, B. N.; Lapyonok, T.; Sinyuk, A.; Mishchenko, M. I.; Yang, P.; Slutsker, I. Non-spherical Aerosol Retrieval Method Employing Light Scattering by Spheroids. *Geophys. Res. Lett.* **2002**, *29* (10), 54-1.

(31) Okada, Y. Numerical Simulations of Light Scattering and Absorption Characteristics of Aggregates. In *Light Scattering Reviews 5*; Kokhanovsky, A. A., Ed.; Springer Berlin Heidelberg: Berlin, Heidelberg, 2010; pp 3−35.

(32) Purcell, E. M.; Pennypacker, C. R. Scattering and Absorption of Light by Nonspherical Dielectric Grains. *Astrophys. J.* **1973**, *186*, 705.
(33) Draine, B. T. The Discrete-Dipole Approximation and Its Application to Interstellar Graphite Grains. *Astrophys. J.* **1988**, *333*, 848.
(34) Pathak, B.; Borah, D.; Khataniar, A.; Bhuyan, P. K.; Buragohain, A. K. Characterization of Bioaerosols in Northeast India in Terms of Culturable Biological Entities along with Inhalable, Thoracic and Alveolar Particles. *J. Earth Syst. Sci.* **2020**, *129* (1), 141.
(35) Pathak, B.; Khataniar, A.; Das, B.; Upadhyaya, S.; Medhi, A.; Bhuyan, P. K.; Buragohain, A. K.; Borah, D. Spatio-Temporal Diversity of Biological Aerosols over Northeast India: A Metagenomic Approach. *Environ. Sci. Pollut. Res.* **2022**, *29* (42), 64096−64111.
(36) Bharali, C.; Pathak, B.; Bhuyan, P. K. Spring and Summer Night-Time High Ozone Episodes in the Upper Brahmaputra Valley of North East India and Their Association with Lightning. *Atmos. Environ.* **2015**, *109*, 234−250.
(37) Bhuyan, P. K.; Bharali, C.; Pathak, B.; Kalita, G. The Role of Precursor Gases and Meteorology on Temporal Evolution of O3 at a Tropical Location in Northeast India. *Environ. Sci. Pollut. Res.* **2014**, *21* (10), 6696−6713.
(38) Pathak, B.; Chutia, L.; Bharali, C.; Bhuyan, P. K. Continental Export Efficiencies and Delineation of Sources for Trace Gases and Black Carbon in North-East India: Seasonal Variability. *Atmos. Environ.* **2016**, *125*, 474−485.
(39) Pathak, B.; Bhuyan, P. K. Characteristics of Atmospheric Pollutants over the Northeastern Region of India. In *Asian Atmospheric Pollution*; Elsevier, 2022; pp 367−392.
(40) Bhuyan, P. K.; Gogoi, M. M.; Moorthy, K. K. Spectral and Temporal Characteristics of Aerosol Optical Depth over a Wet Tropical Location in North East India. *Adv. Space Res.* **2005**, *35* (8), 1423−1429.
(41) Gogoi, M. M.; Bhuyan, P. K.; Krishna Moorthy, K. Estimation of the Effect of Long-Range Transport on Seasonal Variation of Aerosols over Northeastern India. *Ann. Geophys.* **2008**, *26* (6), 1365−1377.
(42) Gogoi, M. M.; Bhuyan, P. K.; Moorthy, K. K. An Investigation of Aerosol Size Distribution Properties at Dibrugarh: North-Eastern India. *Terr. Atmospheric Ocean. Sci.* **2009**, *20* (3), 521.
(43) Gogoi, M. M.; Babu, S. S.; Moorthy, K. K.; Bhuyan, P. K.; Pathak, B.; Subba, T.; Chutia, L.; Kundu, S. S.; Bharali, C.; Borgohain, A.; Guha, A.; De, B. K.; Singh, B.; Chin, M. Radiative Effects of Absorbing Aerosols over Northeastern India: Observations and Model Simulations. *J. Geophys. Res. Atmospheres* **2017**, *122* (2), 1132−1157.
(44) Pathak, B.; Kalita, G.; Bhuyan, K.; Bhuyan, P. K.; Moorthy, K. K. Aerosol Temporal Characteristics and Its Impact on Shortwave Radiative Forcing at a Location in the Northeast of India. *J. Geophys. Res. Atmospheres* **2010**, *115* (D19), 2009JD013462.
(45) Pathak, B.; Bhuyan, P. K.; Gogoi, M.; Bhuyan, K. Seasonal Heterogeneity in Aerosol Types over Dibrugarh-North-Eastern India. *Atmos. Environ.* **2012**, *47*, 307−315.
(46) Pathak, B.; Bhuyan, P. K.; Biswas, J.; Takemura, T. Long Term Climatology of Particulate Matter and Associated Microphysical and Optical Properties over Dibrugarh, North-East India and Inter-Comparison with SPRINTARS Simulations. *Atmos. Environ.* **2013**, *69*, 334−344.
(47) Pathak, B.; Biswas, J.; Bharali, C.; Bhuyan, P. K. Short Term Introduction of Pollutants into the Atmosphere at a Location in the Brahmaputra Basin: A Case Study. *Atmospheric Pollut. Res.* **2015**, *6* (2), 220−229.
(48) Pathak, B.; Subba, T.; Dahutia, P.; Bhuyan, P. K.; Moorthy, K. K.; Gogoi, M. M.; Babu, S. S.; Chutia, L.; Ajay, P.; Biswas, J.; Bharali, C.; Borgohain, A.; Dhar, P.; Guha, A.; De, B. K.; Banik, T.; Chakraborty, M.; Kundu, S. S.; Sudhakar, S.; Singh, S. B. Aerosol Characteristics in North-East India Using ARFINET Spectral Optical Depth Measurements. *Atmos. Environ.* **2016**, *125*, 461−473.
(49) Pathak, B.; Bhuyan, P. K. Absorbing and Scattering Properties of Boundary Layer Aerosols over Dibrugarh, Northeast India. *Int. J. Remote Sens.* **2014**, *35* (14), 5527−5543.
(50) Pathak, B.; Bhuyan, P. K. Climatology of Columnar Aerosol Properties at a Continental Location in the Upper Brahmaputra Basin of North East India: Diurnal Asymmetry and Association with Meteorology. *Adv. Space Res.* **2015**, *56* (7), 1469−1484.
(51) Subba, T.; Gogoi, M. M.; Pathak, B. P. A.; Bhuyan, P. K.; Bhuyan, P. K.; Solmon, F. Assessment of 1D and 3D Model Simulated Radiation Flux Based on Surface Measurements and Estimation of Aerosol Forcing and Their Climatological Aspects. *Atmospheric Res.* **2018**, *204*, 110−127.
(52) Subba, T.; Pathak, B.; Gogoi, M. M.; Ajay, P.; Dahutia, P.; Chakraborty, A.; Bhuyan, P. K. Observations on the Decadal Variability of Aerosol in Eastern Himalayan Foothills: Evidence of an Anthropologically Induced Positive Shift. *Atmos. Environ.* **2023**, *299*, 119638.
(53) Biswas, J.; Pathak, B.; Patadia, F.; Bhuyan, P. K.; Gogoi, M. M.; Babu, S. S. Satellite-retrieved Direct Radiative Forcing of Aerosols over North-east India and Adjoining Areas: Climatology and Impact Assessment. *Int. J. Climatol.* **2017**, *37* (S1), 298−317.
(54) Dahutia, P.; Pathak, B.; Bhuyan, P. K. Aerosols Characteristics, Trends and Their Climatic Implications over Northeast India and Adjoining South Asia. *Int. J. Climatol.* **2018**, *38* (3), 1234−1256.
(55) Dahutia, P.; Pathak, B.; Bhuyan, P. K. Vertical Distribution of Aerosols and Clouds over North-Eastern South Asia: Aerosol-Cloud Interactions. *Atmos. Environ.* **2019**, *215*, 116882.
(56) Pathak, B.; Borgohain, A.; Bhuyan, P. K.; Kundu, S. S.; Sudhakar, S.; Gogoi, M. M.; Takemura, T. Spatial Heterogeneity in near Surface Aerosol Characteristics across the Brahmaputra Valley. *J. Earth Syst. Sci.* **2014**, *123* (4), 651−663.
(57) Borgohain, A.; Kundu, S. S.; Barman, N.; Raju, P. L. N.; Roy, R.; Saha, B.; Ajay, P.; Pathak, B.; Bhuyan, P. K. Investigation of Physical and Optical Properties of Aerosol over High Altitude Stations along the Sub-Himalayan Region of North-Eastern India. *Atmospheric Pollut. Res.* **2020**, *11* (2), 383−392.
(58) Saikia, A.; Pathak, B.; Singh, P.; Bhuyan, P. K.; Adhikary, B. Multi-Model Evaluation of Meteorological Drivers, Air Pollutants and Quantification of Emission Sources over the Upper Brahmaputra Basin. *Atmosphere* **2019**, *10* (11), 703.
(59) Chutia, L.; Ojha, N.; Girach, I. A.; Sahu, L. K.; Alvarado, L. M. A.; Burrows, J. P.; Pathak, B.; Bhuyan, P. K. Distribution of Volatile Organic Compounds over Indian Subcontinent during Winter: WRF-Chem Simulation versus Observations. *Environ. Pollut.* **2019**, *252*, 256−269.
(60) Chutia, L.; Ojha, N.; Girach, I. A.; Pathak, B.; Sahu, L. K.; Bhuyan, P. K. Distribution of Sulfur Dioxide over Indian Subcontinent: Remote Sensing Observations and Model Reanalysis. In *2020 Xxxiiird General Assembly and Scientific Symposium of the International Union of Radio Science*; IEEE: Rome, Italy, 2020; pp 1−4.
(61) Ajay, P.; Pathak, B.; Solmon, F.; Bhuyan, P. K.; Giorgi, F. Obtaining Best Parameterization Scheme of RegCM 4.4 for Aerosols and Chemistry Simulations over the CORDEX South Asia. *Clim. Dyn.* **2019**, *53* (1−2), 329−352.
(62) Ajay, P.; Pathak, B.; Bhuyan, P.; Solmon, F.; Giorgi, F. Sectoral Emissions Contributions to Anthropogenic Aerosol Scenarios over the Indian Subcontinent and Effects of Mitigation on Air Quality, Climate, and Health. *Clim. Res.* **2021**, *85*, 21−33.
(63) Das, S.; Tomar, C. S.; Saha, D.; Shaw, S. O.; Singh, C. Trends in Rainfall Patterns over North-East India during 1961−2010. *Int. J. Earth Atmos Sci.* **2015**, *2*, 37.
(64) India Meteorological Department. *Report on Northeast Monsoon—2018*, 2018. https://mausam.imd.gov.in/chennai/mcdata/ne_monsoon_2018.pdf.
(65) Pathak, B.; Khataniar, A.; Das, B.; Upadhyaya, S.; Medhi, A.; Bhuyan, P. K.; Buragohain, A. K.; Borah, D. Characterization of Biological Aerosols over Northeast India: A Metagenomic Approach. *Research Square* **2021**, 1081395.

https://doi.org/10.1021/acsearthspacechem.5c00197
ACS Earth Space Chem. XXXX, XXX, XXX−XXX

(66) Draine, B. T.; Flatau, P. J. Discrete-Dipole Approximation for Scattering Calculations. *J. Opt. Soc. Am. A* **1994**, *11* (4), 1491.
(67) D'Almeida, G. A.; Koepke, P.; Shettle, E. P. *Atmospheric Aerosols: Global Climatology and Radiative Characteristics*; A. Deepak Pub.: Hampton, Va., USA, 1991; p 1991.
(68) Goudie, A. S.; Middleton, N. J. *Desert Dust in the Global System*; Springer Berlin Heidelberg, 2006.
(69) Chueinta, W.; Hopke, P. K.; Paatero, P. Investigation of Sources of Atmospheric Aerosol at Urban and Suburban Residential Areas in Thailand by Positive Matrix Factorization. *Atmos. Environ.* **2000**, *34* (20), 3319−3329.
(70) Stone, E. A.; Schauer, J. J.; Pradhan, B. B.; Dangol, P. M.; Habib, G.; Venkataraman, C.; Ramanathan, V. Characterization of Emissions from South Asian Biofuels and Application to Source Apportionment of Carbonaceous Aerosol in the Himalayas. *J. Geophys. Res. Atmospheres* **2010**, *115* (D6), 2009JD011881.
(71) He, M.; Wang, X.; Wu, F.; Fu, Z. Antimony Pollution in China. *Sci. Total Environ.* **2012**, *421*−*422*, 41−50.
(72) Maria, S. F.; Russell, L. M.; Turpin, B. J.; Porcja, R. J. FTIR Measurements of Functional Groups and Organic Mass in Aerosol Samples over the Caribbean. *Atmos. Environ.* **2002**, *36* (33), 5185−5196.
(73) Russell, L. M.; Maria, S. F.; Myneni, S. C. B. Mapping Organic Coatings on Atmospheric Particles. *Geophys. Res. Lett.* **2002**, *29* (16), 26-1.
(74) Allen, D. T.; Palen, E. J.; Haimov, M. I.; Hering, S. V.; Young, J. R. Fourier Transform Infrared Spectroscopy of Aerosol Collected in a Low Pressure Impactor (LPI/FTIR): Method Development and Field Calibration. *Aerosol Sci. Technol.* **1994**, *21* (4), 325−342.
(75) Simonsen, M. E.; Sønderby, C.; Li, Z.; Søgaard, E. G. XPS and FT-IR Investigation of Silicate Polymers. *J. Mater. Sci.* **2009**, *44* (8), 2079−2088.
(76) Bahadur, R.; Uplinger, T.; Russell, L. M.; Sive, B. C.; Cliff, S. S.; Millet, D. B.; Goldstein, A.; Bates, T. S. Phenol Groups in Northeastern U.S. Submicrometer Aerosol Particles Produced from Seawater Sources. *Environ. Sci. Technol.* **2010**, *44* (7), 2542−2548.
(77) Simão, J.; Ruiz-Agudo, E.; Rodriguez-Navarro, C. Effects of Particulate Matter from Gasoline and Diesel Vehicle Exhaust Emissions on Silicate Stones Sulfation. *Atmos. Environ.* **2006**, *40* (36), 6905−6917.
(78) Coury, C.; Dillner, A. M. A Method to Quantify Organic Functional Groups and Inorganic Compounds in Ambient Aerosols Using Attenuated Total Reflectance FTIR Spectroscopy and Multivariate Chemometric Techniques. *Atmos. Environ.* **2008**, *42* (23), 5923−5932.
(79) Colthup, N. B.; Daly, L. H.; Wiberley, S. E. *Introduction to Infrared and Raman Spectroscopy*, 3rd ed.; Academic Press Inc., New York., 1990.
(80) Matthias-Maser, S.; Jaenicke, R. Examination of Atmospheric Bioaerosol Particles with Radii > 0.2 Mm. *J. Aerosol Sci.* **1994**, *25* (8), 1605−1613.
(81) Coz, E.; Artíñano, B.; Clark, L. M.; Hernandez, M.; Robinson, A. L.; Casuccio, G. S.; Lersch, T. L.; Pandis, S. N. Characterization of Fine Primary Biogenic Organic Aerosol in an Urban Area in the Northeastern United States. *Atmos. Environ.* **2010**, *44* (32), 3952−3962.
(82) Van Malderen, H.; Van Grieken, R.; Khodzher, T.; Obolkin, V.; Potemkin, V. Composition of Individual Aerosol Particles above Lake Baikal, Siberia. *Atmos. Environ.* **1996**, *30* (9), 1453−1465.
(83) Cong, Z.; Kang, S.; Dong, S.; Zhang, Y. Individual Particle Analysis of Atmospheric Aerosols at Nam Co, Tibetan Plateau. *Aerosol Air Qual. Res.* **2009**, *9* (3), 323−331.
(84) Kim, H.; Kim, D.-U.; Lee, H.; Yun, J.; Ka, J.-O. Syntrophic Biodegradation of Propoxur by Pseudaminobacter Sp. SP1a and Nocardioides Sp. SP1b Isolated from Agricultural Soil. *Int. Biodeterior. Biodegrad.* **2017**, *118*, 1−9.
(85) Zhang, Q.; Jimenez, J. L.; Canagaratna, M. R.; Allan, J. D.; Coe, H.; Ulbrich, I.; Alfarra, M. R.; Takami, A.; Middlebrook, A. M.; Sun, Y. L.; Dzepina, K.; Dunlea, E.; Docherty, K.; DeCarlo, P. F.; Salcedo, D.; Onasch, T.; Jayne, J. T.; Miyoshi, T.; Shimono, A.; Hatakeyama, S.; Takegawa, N.; Kondo, Y.; Schneider, J.; Drewnick, F.; Borrmann, S.; Weimer, S.; Demerjian, K.; Williams, P.; Bower, K.; Bahreini, R.; Cottrell, L.; Griffin, R. J.; Rautiainen, J.; Sun, J. Y.; Zhang, Y. M.; Worsnop, D. R. Ubiquity and Dominance of Oxygenated Species in Organic Aerosols in Anthropogenically-influenced Northern Hemisphere Midlatitudes. *Geophys. Res. Lett.* **2007**, *34* (13), 2007GL029979.
(86) Cong, Z.; Kang, S.; Liu, X.; Wang, G. Elemental Composition of Aerosol in the Nam Co Region, Tibetan Plateau, during Summer Monsoon Season. *Atmos. Environ.* **2007**, *41* (6), 1180−1187.
(87) U.S. Geological Survey. *Geological Survey Research 1976; Professional Paper*; US Geological Survey, 1976.
(88) Gugamsetty, B.; Wei, H.; Liu, C.-N.; Awasthi, A.; Hsu, S.-C.; Tsai, C.-J.; Roam, G.-D.; Wu, Y.-C.; Chen, C.-F. Source Characterization and Apportionment of PM10, PM2.5 and PM0.1 by Using Positive Matrix Factorization. *Aerosol Air Qual. Res.* **2012**, *12* (4), 476−491.
(89) Duce, R. A.; Hoffman, G. L.; Zoller, W. H. Atmospheric Trace Metals at Remote Northern and Southern Hemisphere Sites: Pollution or Natural? *Science* **1975**, *187* (4171), 59−61.
(90) Zoller, W. H.; Gladney, E. S.; Duce, R. A. Atmospheric Concentrations and Sources of Trace Metals at the South Pole. *Science* **1974**, *183* (4121), 198−200.
(91) Lee, J. D. *Concise Inorganic Chemistry*; Chapman and Hall Ltd, 1993.
(92) Thorpe, A.; Harrison, R. M. Sources and Properties of Non-Exhaust Particulate Matter from Road Traffic: A Review. *Sci. Total Environ.* **2008**, *400* (1−3), 270−282.
(93) Querol, X.; Alastuey, A.; Viana, M.; Moreno, T.; Reche, C.; Minguillón, M. C.; Ripoll, A.; Pandolfi, M.; Amato, F.; Karanasiou, A.; Pérez, N.; Pey, J.; Cusack, M.; Vázquez, R.; Plana, F.; Dall'Osto, M.; De La Rosa, J.; Sánchez De La Campa, A.; Fernández-Camacho, R.; Rodríguez, S.; Pio, C.; Alados-Arboledas, L.; Titos, G.; Artíñano, B.; Salvador, P.; García Dos Santos, S.; Fernández Patier, R. Variability of Carbonaceous Aerosols in Remote, Rural, Urban and Industrial Environments in Spain: Implications for Air Quality Policy. *Atmospheric Chem. Phys.* **2013**, *13* (13), 6185−6206.
(94) Amato, F.; Pandolfi, M.; Escrig, A.; Querol, X.; Alastuey, A.; Pey, J.; Perez, N.; Hopke, P. K. Quantifying Road Dust Resuspension in Urban Environment by Multilinear Engine: A Comparison with PMF2. *Atmos. Environ.* **2009**, *43* (17), 2770−2780.
(95) Zhao, Z.; Cao, J.; Shen, Z.; Xu, B.; Zhu, C.; Chen, L. -A.; Su, X.; Liu, S.; Han, Y.; Wang, G.; Ho, K. Aerosol Particles at a High-altitude Site on the Southeast Tibetan Plateau, China: Implications for Pollution Transport from South Asia. *J. Geophys. Res. Atmospheres* **2013**, *118* (19), 11360.
(96) Engelbrecht, J. P.; McDonald, E. V.; Gillies, J. A.; Jayanty, R. K. M.; Casuccio, G.; Gertler, A. W. Characterizing Mineral Dusts and Other Aerosols from the Middle East—Part 1: Ambient Sampling. *Inhal. Toxicol.* **2009**, *21* (4), 297−326.
(97) Snyder, C. S.; Bruulsema, T. W.; Jensen, T. L.; Fixen, P. E. Review of Greenhouse Gas Emissions from Crop Production Systems and Fertilizer Management Effects. *Agric. Ecosyst. Environ.* **2009**, *133* (3−4), 247−266.
(98) Haywood, J.; Boucher, O. Estimates of the Direct and Indirect Radiative Forcing Due to Tropospheric Aerosols: A Review. *Rev. Geophys.* **2000**, *38* (4), 513−543.
(99) Sumlin, B. J.; Heinson, Y. W.; Shetty, N.; Pandey, A.; Pattison, R. S.; Baker, S.; Hao, W. M.; Chakrabarty, R. K. UV−Vis−IR Spectral Complex Refractive Indices and Optical Properties of Brown Carbon Aerosol from Biomass Burning. *J. Quant. Spectrosc. Radiat. Transfer* **2018**, *206*, 392−398.
(100) Chartier, R. T.; Greenslade, M. E. Initial Investigation of the Wavelength Dependence of Optical Properties Measured with a New Multi-Pass Aerosol Extinction Differential Optical Absorption Spectrometer (AE-DOAS). *Atmospheric Meas. Technol.* **2012**, *5* (4), 709−721.

https://doi.org/10.1021/acsearthspacechem.5c00197
ACS Earth Space Chem. XXXX, XXX, XXX−XXX

(101) Nousiainen, T.; Zubko, E.; Lindqvist, H.; Kahnert, M.; Tyynelä, J. Comparison of Scattering by Different Nonspherical, Wavelength-Scale Particles. *J. Quant. Spectrosc. Radiat. Transfer* **2012**, *113* (18), 2391−2405.
(102) Alfaro, S. C.; Lafon, S.; Rajot, J. L.; Formenti, P.; Gaudichet, A.; Maillé, M. Iron Oxides and Light Absorption by Pure Desert Dust: An Experimental Study. *J. Geophys. Res. Atmospheres* **2004**, *109* (D8), 2003JD004374.
(103) Akimov, Y. A. Mie Scattering Theory: A Review of Physical Features and Limitations. *arXiv* **2024**, arXiv:2401.04146.
(104) Yang, P.; Feng, Q.; Hong, G.; Kattawar, G. W.; Wiscombe, W. J.; Mishchenko, M. I.; Dubovik, O.; Laszlo, I.; Sokolik, I. N. Modeling of the Scattering and Radiative Properties of Nonspherical Dust-like Aerosols. *J. Aerosol Sci.* **2007**, *38* (10), 995−1014.

https://doi.org/10.1021/acsearthspacechem.5c00197
ACS Earth Space Chem. XXXX, XXX, XXX−XXX